Alonso, E., L. R. Alejano, F. Varas, G. Fdez-Manín, and C. Carranza-Torres (2003). Ground response curves for rock masses exhibiting strain-softening behaviour. *Int. J. Numer. Anal. Meth. Geomech. 27*, 1153–1185.

INTERNATIONAL JOURNAL FOR NUMERICAL AND ANALYTICAL METHODS IN GEOMECHANICS
Int. J. Numer. Anal. Meth. Geomech., 2003; **27**:1153–1185 (DOI: 10.1002/nag.315)

Ground response curves for rock masses exhibiting strain-softening behaviour

E. Alonso[1,†], L. R. Alejano[1,*,‡], F. Varas[2,§], G. Fdez-Manín[2,¶] and C. Carranza-Torres[3,‖]

[1] *Natural Resources and Environmental Engineering Department, University of Vigo. Campus Lagoas-Marcosende, Vigo E-36280, Spain*

[2] *Applied Mathematics Department, University of Vigo, Campus Lagoas-Marcosende, Vigo E-36280, Spain*

[3] *Itasca Consulting Group Inc., 111 Third Avenue, Suite 450, Minneapolis, MN 55401, U.S.A.*

SUMMARY

A literature review has shown that there exist adequate techniques to obtain ground reaction curves for tunnels excavated in elastic-brittle and perfectly plastic materials. However, for strain-softening materials it seems that the problem has not been sufficiently analysed. In this paper, a one-dimensional numerical solution to obtain the ground reaction curve (GRC) for circular tunnels excavated in strain-softening materials is presented.

The problem is formulated in a very general form and leads to a system of ordinary differential equations. By adequately defining a fictitious 'time' variable and re-scaling some variables the problem is converted into an initial value one, which can be solved numerically by a Runge–Kutta–Fehlberg method, which is implemented in MATLAB environment.

The method has been developed for various common particular behaviour models including Tresca, Mohr–Coulomb and Hoek–Brown failure criteria, in all cases with non-associative flow rules and two-segment piecewise linear functions related to a principal strain-dependent plastic parameter to model the transition between peak and residual failure criteria.

Some particular examples for the different failure criteria have been run, which agree well with closed-form solutions—if existing—or with FDM-based code results. Parametric studies and specific charts are created to highlight the influence of different parameters.

The proposed methodology intends to be a wider and general numerical basis where standard and newly featured behaviour modes focusing on obtaining GRC for tunnels excavated in strain-softening materials can be implemented. This way of solving such problems has proved to be more efficient and less time consuming than using FEM- or FDM-based numerical 2D codes. Copyright © 2003 John Wiley & Sons, Ltd.

KEY WORDS: ground response curves; tunnels; strain-softening; self-similarity

*Correspondence to: L. R. Alejano, ETSI Minas, Universidad de Vigo Campus Lagoas-Marcosende, E-36280 Vigo (Pontevedra), Spain.
† E-mail: ealonso@uvigo.es
‡ E-mail: alejano@uvigo.es
§ E-mail: curro@dma.uvigo.es
¶ E-mail: manin@dma.uvigo.es
‖ E-mail: cct@itascacg.com

Contract/grant sponsor: Local Government of Galicia; contract/grant number: PGIDT00PXI32101PR

Received 31 December 2002
Revised 30 June 2003
Accepted 30 June 2003

Published online 26 August 2003

1. INTRODUCTION

The analysis of circular tunnels excavated in elasto-plastic continua under hydrostatic stress fields has been one of the main sources of knowledge and insight as far as ground support principles are concerned. The response of such excavations can be pinpointed in a single curve relating the wall convergence to the internal pressure, which in turn can be related to the distance to the face. This curve is usually known as ground reaction curve. This kind of analysis also permits associating the convergence on the wall to the formation of a plastic aureole around a tunnel of radius R under a hydrostatic field stress of magnitude σ^0 [1–4]. This simple analysis is often used as a point of departure in studying the mechanics of deformation around underground excavations [5].

The basic elements of this concept are illustrated in Figure 1, which shows how the convergence and the extent of the plastic zone can be related to *the internal or equivalent pressure* p_i, also referred to as *support pressure*. In tunnels without support, the excavation process is simulated diminishing the value of this pressure from the far field σ^0 value to null. For unsupported tunnels there is no failure if the hoop stress in the tunnel wall is smaller than the unconfined compressive stress of the rock mass. When the internal pressure attains a critical value, p_i^*, a failure zone of radius R_p, develops around the tunnel, in such a way that this radius increases as far as the internal pressure decreases [2, 3, 6, 7]. However, the so-called yield does not necessarily mean the collapse of the excavation, since the failed rock mass can still possess considerable strength. If the extent of the plastic zone is small in relation to the tunnel size, the only evidence of failure is the occurrence of spalling and/or slabbing locally. But if a larger yielded zone occurs, important displacements towards the tunnel take place and the collapse of the unsupported tunnel is probable.

This technique has proved to be very useful since it can help in the support and/or reinforcement design. This design should take into account the interaction between rock mass and engineered materials used as support or reinforcement. The art of tunnel design is that of finding the right support and/or reinforcement and the right moment to install them. If this is correctly done, uncontrolled displacements of the rock mass or over-stressing on the support system may result in tunnel collapse.

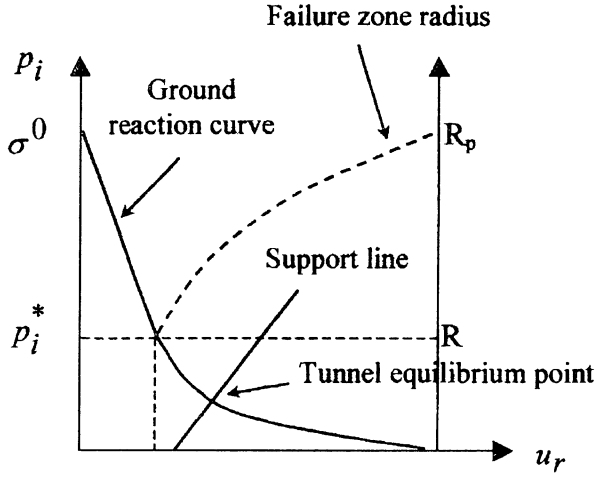

Figure 1. Ground response curve, support characteristic line and failure zone radius.

The stiffness and the distance to the face when installing support and reinforcement are key aspects in displacement control, and in the interacting between rock mass and support. This interaction can be analysed by means of the ground response curve of the rock mass and the support characteristic line. Certainly, the intersection of these two curves (Figure 1) gives the so-called tunnel equilibrium point, where the final displacement of the supported tunnel and the pressure of support can be obtained from a theoretical analysis by projecting this point on the two axes of the GRC. In practice, support stiffness is not usually a constant, and very often the support reaction relationship is non-linear. Also it is not easy to appropriately introduce the behaviour of reinforcement within this technique.

Some weak points of this technique are the following. First, the actual stress path followed by the points around the tunnel is not correctly represented due to the 3D effect [8]. Then, the actual variability of the material behaviour parameters is usually so significant, that results always involve a high degree of uncertainty [9]. Nevertheless, this technique is still having great practical value in engineering, as a method contributing to tunnel design [10].

In order to obtain a realistic ground response curve for a tunnel it is important to start from a precise knowledge of the ground behaviour and their parameters. According to its post-failure behaviour, elasto-plastic materials can be divided into: (i) perfectly brittle, (ii) perfectly plastic or ductile, (iii) strain-softening and (iv) strain-hardening materials. Based on a wide experience in the field of underground rock engineering, Hoek and Brown [11] suggest that average quality rock masses behave in a strain-softening mode, whereas soft rock masses behave in a ductile way and hard rock masses in an elastic-brittle fashion. Even if some researchers [12–14] concluded that strain-softening is not a true intrinsic material property of the rock mass, it has been widely observed [15–17] that beyond the peak strength rock materials experience damage due to micro-cracking and faulting, leading to a strain-softening response.

Most of the existing solutions concerning the calculation of the ground reaction curve for tunnels involve perfectly plastic [3, 4, 7, 10, 18] or perfectly brittle [3, 10, 19–21] behaviour. There are also some solutions concerning strain-softening behaviour [3, 10, 22,23] but they are used to cover restricted cases, for instance, Tresca failure criterion, or they make simplifications in such a way that solutions are not enough rigorous [21].

After a literature review, a set of the most common solutions are presented in Table I, together with the most relevant topics of their formulation, which include rock mass behaviour model, failure criterion, flow rule type and particular features. A similar but older table of this type can be consulted in Reference [22]. This table shows that only a few authors have contemplated the obtaining of GRC for strain softening materials. As far as this review's results indicate only Carranza-Torres [10] and Panet [3] solve the problem for particular cases of strain-softening behaviour and Mohr–Coulomb failure criterion. Whereas Brown *et al.* [22] solve it for strain-softening Hoek–Brown failure criterion and associated flow rule. Finally, Gumusoglu *et al.* [24] solve the problem by means of an FEM-based code for a particular case of Hoek–Brown failure criterion including non-associated flow rule. Even if the solution presented by Brown *et al.* [22] still possesses much rock engineering practical value, it is not strictly rigorous in that the elastic strain increments are not considered within the plastic regime.

As a result of this review, it turns out that there is still not a satisfactory general solution concerning the obtaining of the ground reaction curve for tunnels excavated in strain-softening rock masses. This is surely due to the fact of the non-simple definition of the behaviour model, to the non-existence of closed-form solutions and to the difficulty when dealing with many parameters. It is the main aim of this paper to deepen the understanding of the solution of this

Table I. Ground response curve most commonly used solutions.

Behaviour	Failure criterion	Flow-rule	Reference
Elastic perfectly plastic	Mohr–Coulomb	Associated	[3, 4]
		Non-associated	[10, 18]
	Hoek–Brown	Associated	[7]
		Non-associated	[7]
Elastic perfectly brittle	Mohr–Coulomb	Associated	[3, 23]*,†
		Non-associated	[3, 23]‡,§
	Hoek–Brown	Associated	[19–21]¶
		Non-associated	[21]
Strain softening	Mohr–Coulomb	Associated	[10]‖
		Non-associated	[3]**
	Hoek–Brown	Associated	[22]††
		Non-associated	[24]‡‡

*Residual cohesion and friction different from peak ones.
†Null residual cohesion, residual friction different from peak one.
‡Residual cohesion and friction different from peak ones.
§Null residual cohesion, residual friction different from peak one.
¶Non-linear Fairhurst failure criterion.
‖Null peak and residual friction, or Tresca failure criterion.
**Equal peak and residual friction and null residual cohesion, numerical solution.
††Numerical solution.
‡‡FEM-based solution of a particular case.

problem, by adequately defining a rock mass-oriented strain-softening behaviour and by numerically solving this problem for some relevant cases.

2. STRAIN-SOFTENING BEHAVIOUR

Under this title a rock mass oriented strain-softening behaviour model is presented. This study is founded in the incremental theory of plasticity [25–28], developed in order to model the process of plastic deformation. According to this theory, a material is characterized by a failure criterion f, and a plastic potential, g. One of the main features of this behaviour model is that the failure criterion and the plastic potential do not only depend on the stress tensor σ_{ij}, but also on the so-called plastic or softening parameter η. Then, the behaviour model is plastic strain dependent.

2.1. Failure criterion

The failure criterion is defined as follows:

$$f(\sigma_{ij}, \eta) = 0 \tag{1}$$

The strain-softening behaviour is characterized by a gradual transition from a peak failure criterion to a residual one. This transition is governed by the softening parameter η. In this model, the transition is defined in such a way that the elastic regime exists while the softening parameter is null, the softening regime occurs whenever $0 < \eta < \eta^*$, and the residual state takes

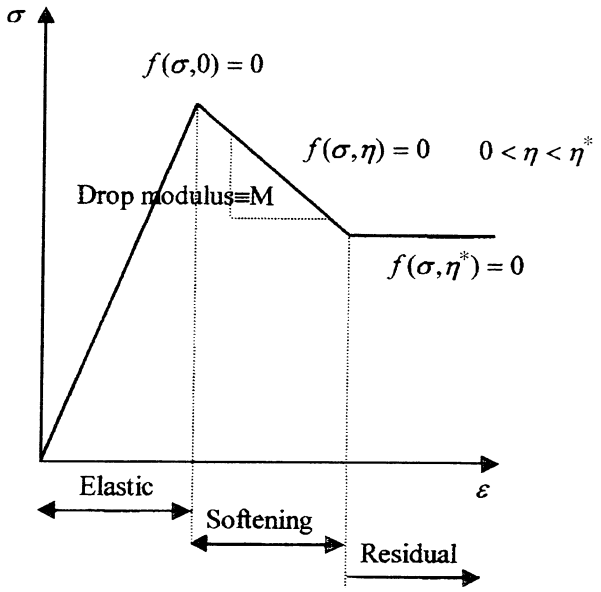

Figure 2. Stress–strain curve of an unconfined test performed on a sample of a strain-softening material.

place when $\eta \geqslant \eta^*$, being defined η^* as the value of the softening parameter controlling the transition between the softening and residual stages.

Figure 2 illustrates this type of strain-softening behaviour for an unconfined compressive test. The slope of the softening stage or drop modulus is denoted by M. If this drop modulus tends to infinity, the perfectly brittle behaviour appears, and if it tends to zero, the perfectly plastic behaviour is obtained. It is clear then that the perfectly brittle or elastic-brittle–plastic and the perfectly plastic behaviour models are limiting cases of this strain-softening model, which can be considered as the most general case.

The behaviour illustrated in Figure 2 serves as a first approach to model the stress–strain behaviour observed in tested rock samples and rock masses. As previously discussed, the actual existence of this type of behaviour is still a controversial topic. But it certainly seems that it is able to represent the macroscopic results commonly observed in practice, even if it is not able to simulate the very complex microscopic phenomena—micro-fracture initiation, propagation and coalescence, damage—which involve the actual processes of rock deformation and failure. Even though the proposed strain-softening behaviour model might not exactly represent the actual rock behaviour, it has been one of the aims of this paper to prepare a numerical basis where further changes could be included, such as stress-dependent elastic modulus or dilation, in order to progressively improve the modelling technique.

2.2. *Plastic potential*

The constitutive equation of a strain-softening material can be obtained according to the incremental theory of plasticity. The plastic strain increments can be obtained from the plastic potential:

$$g(\sigma_{ij}, \eta) \tag{2}$$

according to

$$\dot{\varepsilon}_{ij}^{\mathrm{p}} = \dot{\lambda}\frac{\partial g}{\partial \sigma_{ij}} \tag{3}$$

where $\dot{\lambda}$ is a plastic multiplier and it is unknown. Equation (3) is the constitutive equation of the plastic regime and it is usually called flow rule. If the plastic potential coincides with the failure criterion, then it is called associated flow rule, and if it is not the case, it is called non-associated flow rule. This rule marks the direction of the plastic strain increments. Incremental plasticity involves the consideration of a fictitious 'time' variable, even if it does not have physical meaning. This variable controls the evolution of plasticity. This 'time' variable called τ, controls the plastic strain increments in the following manner:

$$\dot{\varepsilon}_{ij}^{\mathrm{p}} = \frac{\partial \varepsilon_{ij}^{\mathrm{p}}}{\partial \tau} \tag{4}$$

The final constitutive equation of the plastic regime according to Hill [26] is

$$\dot{\sigma}_{ij} = \left[C_{ijkl}^{\mathrm{e}} - \frac{\langle 1\rangle}{H}\left(\frac{\partial g}{\partial \sigma_{mn}} C_{mnij}^{\mathrm{e}} \frac{\partial f}{\partial \sigma_{rs}} C_{rskl}^{\mathrm{e}}\right)\right]\dot{\varepsilon}_{kl} \tag{5}$$

Where $\langle 1\rangle$ stands for 0 or 1, depending on whether the increment is purely elastic ($\dot{\lambda} = 0$) or also contains plastic terms ($\dot{\lambda} > 0$). H is the plastic modulus and it can be subdivided into two, in such a way that $H = H_0 + H_t$; where H_0 coincides with the plastic modulus of the perfectly plastic behaviour and H_t is known as the hardening/softening modulus.

$$H_0 = C_{ijkl}^{\mathrm{e}} \frac{\partial f}{\partial \sigma_{ij}} \frac{\partial g}{\partial \sigma_{kl}}, \quad H_t = -\frac{\partial f}{\partial \eta} \tag{6}$$

Equation (5) is a relation of the type $\dot{\sigma}_{ij} = C_{ijkl}^{\mathrm{ep}} \dot{\varepsilon}_{kl}$. This expression stands whenever C_{ijkl}^{ep} can be written as

$$C_{ijkl}^{\mathrm{ep}} = C_{ijkl}^{\mathrm{e}} - \frac{\langle 1\rangle}{H} \frac{\partial g}{\partial \sigma_{mn}} C_{mnij}^{\mathrm{e}} \frac{\partial f}{\partial \sigma_{rs}} C_{rskl}^{\mathrm{e}} = C_{ijkl}^{\mathrm{e}} + C_{ijkl}^{\mathrm{p}} \tag{7}$$

where C_{ijkl}^{e} is a symmetric matrix ($C_{ijkl}^{\mathrm{e}} = C_{klij}^{\mathrm{e}}$) and C_{ijkl}^{ep} is not generally a symmetric matrix, but it is in the case of associated flow rule, which involves that $\partial f/\partial \sigma_{ij} = \partial g/\partial \sigma_{ij}$ and therefore $C_{ijkl}^{\mathrm{ep}} = C_{klij}^{\mathrm{ep}}$.

2.3. *Softening parameter*

If a strain-softening behaviour model as the one defined is considered, the softening parameter η controls the strength capacity between the peak and the residual failure criteria. Hence, a value of this parameter equal to η^* produces the transition between the softening and residual regimes. This parameter η can be defined in different ways, but so far there has not been a wide support among researchers for any of its possible forms. There are two different common ways of defining this parameter. First [29] it is defined as a function of internal variables, whereas according to the second method [30] it is defined in an incremental way. In the former case, based on internal variables, the most utilized plastic parameter is that obtained as the difference between the major and minor principal plastic strains, which reflects the plastic shear strain:

$$\eta = \gamma^{\mathrm{p}} = \varepsilon_1^{\mathrm{p}} - \varepsilon_3^{\mathrm{p}} \tag{8}$$

This plastic parameter will be chosen for the development of the studies presented in this paper.

For the latter, we can find in literature incremental softening parameters $\dot{\eta}$ [30] depending on plastic strain increments, being the most common defined as

$$\dot{\eta} = \frac{\Delta\eta}{\Delta\tau} = \sqrt{\tfrac{2}{3}[\dot{\varepsilon}_1^{\mathrm{p}}\dot{\varepsilon}_1^{\mathrm{p}} + \dot{\varepsilon}_2^{\mathrm{p}}\dot{\varepsilon}_2^{\mathrm{p}} + \dot{\varepsilon}_3^{\mathrm{p}}\dot{\varepsilon}_3^{\mathrm{p}}]} \tag{9}$$

Code FLAC-2D, which will be used later in this study, implements an incremental plastic parameter e^{ps} of the second type, whose incremental form is [31]:

$$\Delta e^{\mathrm{ps}} = \left\{\tfrac{1}{2}(\Delta\varepsilon_1^{\mathrm{ps}} - \Delta\varepsilon_m^{\mathrm{ps}})^2 + \tfrac{1}{2}(\Delta\varepsilon_m^{\mathrm{ps}})^2 + \tfrac{1}{2}(\Delta\varepsilon_3^{\mathrm{ps}} - \Delta\varepsilon_m^{\mathrm{ps}})^2\right\}^{1/2} \tag{10}$$

where, $\Delta\varepsilon_m^{\mathrm{ps}} = \frac{1}{3}(\Delta\varepsilon_1^{\mathrm{ps}} + \Delta\varepsilon_3^{\mathrm{ps}})$ and $\Delta\varepsilon_j^{\mathrm{ps}}$ $j = 1, 2, 3$ are the principal increments of the shear plastic strain. This incremental plastic parameter can be, however, related to the more standard γ^{p} or plastic shear strain. If an elasto-plastic strain-softening material with constant dilation angle is considered, characterized by a plastic potential $g = \sigma_1 - K_\psi\sigma_3$, where $K_\psi = (1 + \sin\psi)/(1 - \sin\psi)$, then the following relationship between γ^{p} and η_{FLAC} can be deduced:

$$\eta_{\mathrm{FLAC}} = \frac{\sqrt{3}}{3}\sqrt{1 + K_\psi + K_\psi^2}\,\frac{\gamma^{\mathrm{p}}}{1 + K_\psi} \tag{11}$$

The reader can check how for null dilation, as proposed by some authors [11] for particular rock masses, it occurs that $\eta_{\mathrm{FLAC}} = \gamma^{\mathrm{p}}/2$. Figure 3 illustrates the relationship of Equation (11) for two different dilation angle values. It can be observed that even for high dilation angle values, the final relationship between plastic parameters is quite close to that of null dilation.

Some authors [32] think that the softening parameter should be attached to the type of test more than to the material itself. Others think that it marks quite definitely the post-failure behaviour of materials. For instance Pethukov and Linkov [33] think that this parameter may control the ability of rock bursting of pillars. Studying data from different authors [11, 29, 34] concerning rock masses, in situ and numerical data of coal pillars and tests on different size coal

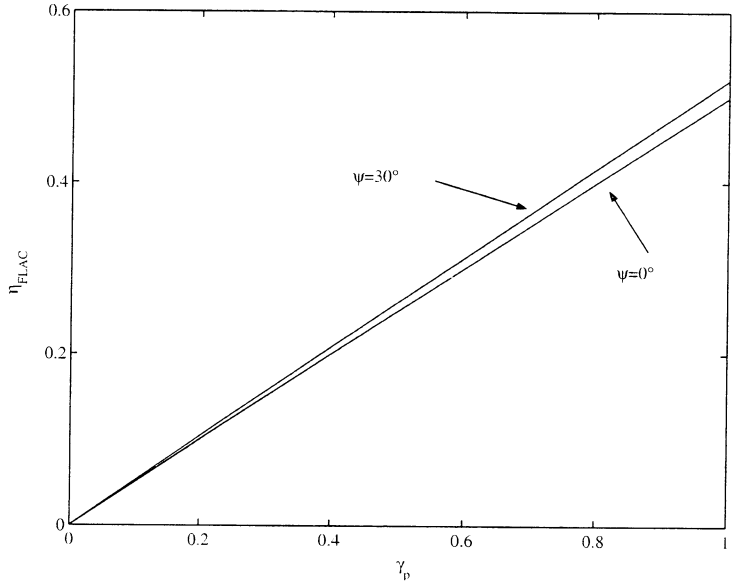

Figure 3. Relationship between FLACs softening parameter and $\gamma^{\mathrm{p}} = \varepsilon_1^{\mathrm{p}} - \varepsilon_3^{\mathrm{p}}$ for constant dilation.

samples, it seems that the critical value of the softening parameter γ^p may vary between 0.01 and 0.001—1 and 0.1%.

3. PROBLEM FORMULATION

The so-called rock-support interaction analysis [1, 3, 4, 10, 19, 20] is based on the calculation of the ground reaction curve and the support characteristic line. It studies the radial displacements in the excavation wall and the extent of the plastic zone around it by means of solving a sequence of 2D problems corresponding to decreasing pressures—from the field stress to zero—on the excavation boundary. From a computational point of view the solution of this sequence of problems is much less time consuming than the corresponding 3D solution, offering a simple and rather useful technique for tunnel design.

In order to solve this problem a number of simplifying assumptions have to be made due to the large number of factors that should be taken into account. In this study the classical basic hypotheses [3, 4, 10, 19, 20] are made.

The formulation of this problem is firstly based on the equilibrium equation. In plane-strain conditions and taking into account radial symmetry it can be written in cylindrical co-ordinates as follows:

$$\frac{\partial \sigma_r}{\partial r} + \frac{\sigma_r - \sigma_\theta}{r} = 0 \tag{12}$$

The following equation that has to be applied is that of persistence—also called active plasticity condition—which implies that, once attained the plastic state, the material should keep on the failure criterion function. This means that the point of co-ordinates $(r, \tau + \Delta\tau)$ always satisfies the failure criterion. So $\dot{f} = 0$, and for the previously presented behaviour model:

$$\frac{\partial f}{\partial \sigma_r}\frac{\partial \sigma_r}{\partial \tau} + \frac{\partial f}{\partial \sigma_\theta}\frac{\partial \sigma_\theta}{\partial \tau} + \frac{\partial f}{\partial \eta}\frac{\partial \eta}{\partial \tau} = 0 \tag{13}$$

Finally the flow rule is considered (3). This law governs the behaviour of the material in the plastic state, in such a way that the rates of the plastic strain can be derived from Equation (3), once the plastic potential is defined. For the case of a circular excavation, the principal strains are the hoop and radial strains and the hoop and radial strain rates are:

$$\dot{\varepsilon}_r = \frac{\partial \varepsilon_r}{\partial \tau}, \quad \dot{\varepsilon}_\theta = \frac{\partial \varepsilon_\theta}{\partial \tau} \tag{14}$$

The strain–displacement equations in the case of plane-strain and radial symmetry are:

$$\dot{\varepsilon}_\theta = \frac{v_r}{r} \tag{15a}$$

$$\dot{\varepsilon}_r = \frac{\partial v_r}{\partial r} \tag{15b}$$

$$v_r = \frac{\partial u_r}{\partial \tau} \tag{15c}$$

Eliminating the plastic multiplier from the flow rule (3) and formulae (14), breaking down the strain rates in their elastic and plastic parts and introducing (15c), the constitutive equation of

the plastic state is obtained as

$$\frac{\partial v_r}{\partial r} - A_1 \frac{v_r}{r} = \frac{1}{2G}[A_2\dot{\sigma}_r - A_3\dot{\sigma}_\theta]$$
$$A_1 = \frac{\partial g}{\partial \sigma_r}\left(\frac{\partial g}{\partial \sigma_\theta}\right)^{-1}, \quad A_2 = 1 + v(A_1 - 1), \quad A_3 = A_1(1 - v) + v \tag{16}$$

Equations (12), (13), (15c) and (16) form the system of partial differential equations to be solved. The solution should provide the values of the hoop and radial stresses and the radial displacements. It is important to highlight that the displacements and stresses depend on two factors: on a physical variable r, which is the distance to the centre of the excavation, and on a fictitious 'time' variable τ, which is a measurement of the plasticity evolution. The aforementioned radial displacement and radial and hoop stress are then written $u_r(r,\tau)$, $\sigma_r(r,\tau)$ and $\sigma_\theta(r,\tau)$, respectively.

The boundary conditions associated to this problem are:

$$\lim_{r\to+\infty} \sigma_r(r,\tau) = \lim_{r\to+\infty} \sigma_\theta(r,\tau) = \sigma^0$$
$$\sigma_r(R,\tau) = p_i \tag{17}$$

where R represents the tunnel radius, p_i the pressure on the excavation wall and σ^0 the field stress. Since the radial stress and the radial strain rate are generally continuous, they can be computed in the elastic region, and then, they can be used to integrate the equations in the plastic side of the interface.

For the particular case of elastic-brittle behaviour, characterized by a sudden loss of strength once attained the elastic limit [35], the boundary condition concerning strain rate should be carefully studied due to the fact that a velocity jump takes place in the elasto-plastic interface [10].

Replacing the asymptotic boundary conditions by the elasto-plastic interface conditions, the reformulated boundary conditions stand:

$$\sigma_r(R_p,\tau) = p_i^*$$
$$\sigma_\theta(R_p,\tau) = 2\sigma^0 - p_i^* \tag{18}$$
$$u_r(R_p,\tau) = \frac{\sigma^0 - p_i^*}{2G} R_p$$

where p_i^* represents radial stress at the elasto-plastic interface, obtained from the intersection of the elastic solution with the failure criterion (as Figure 4 illustrates), R_p is the radius of the plastic zone and G is the shear modulus of the material.

The system of equations is going to be solved from $r = R_p$ up to R_p^*, in such a way that:

$$\eta(R_p^*) = \eta^* \tag{19}$$

Starting from this value, the transition to the residual state takes place, and the equations are solved for $\eta = \eta^*$ (taking as conditions the values obtained for $r = R_p^*$ when solving the softening regime). The residual zone is solved up to $r = R$, where it should be imposed that $\sigma_r(R) = p_i$. The solution of the residual regime is meaningful whenever $\sigma_r(R_p^*) > p_i$, otherwise there would only be a softening regime zone (Figure 4). The transition from the softening to the residual regime

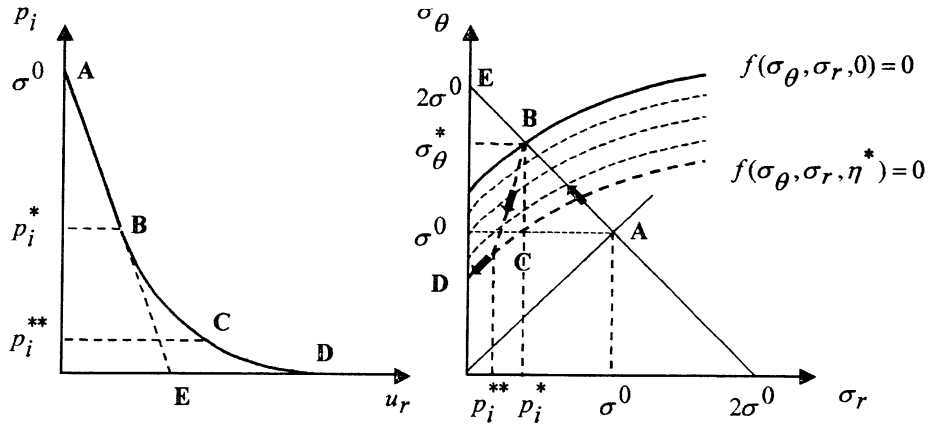

Figure 4. Ground reaction curve—left hand side and stress path of the unloading process (ABCD)—right hand side. The general strain-softening behaviour case is presented, which includes not only a softening zone (BC) but also the development of a residual zone (CD).

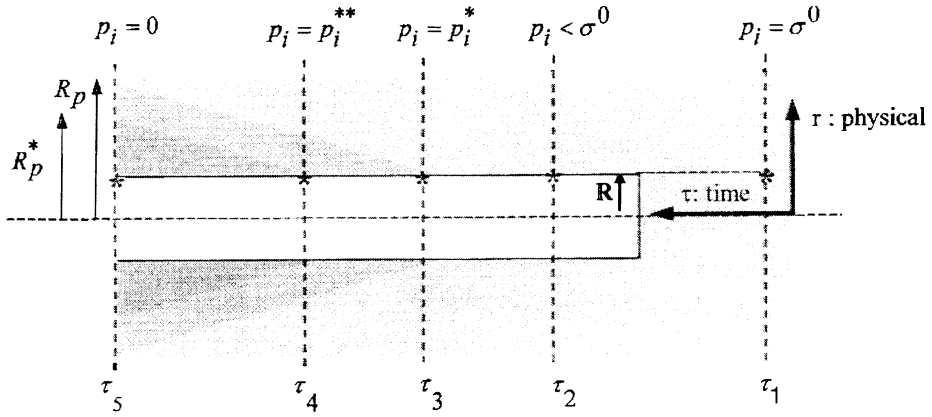

Figure 5. Evolution of the plastic zone within the fictitious time also denoted variable τ.

takes place for a value of the internal pressure p_i^{**}, which can be obtained as the intersection of the softening solution and the residual failure criterion.

The fictitious time variable controls the evolution of the plastic zone (see Figure 5). It does so in such a way that solutions should be imposed to start from the elastic regime—for an internal pressure equal to the field stress, associated to a fictitious time τ_1. Then, they continue being elastic for an internal pressure smaller than the field stress for τ_2, until the first yield appears for a critical value of the internal pressure p_i^* for τ_3. The extent of the plastic zone will increase as far as the internal pressure is reduced up to zero and fictitious time elapses.

The problem to be solved is then formulated by the system of partial differential equations ((12), (13), (15c) and (16)) together with the boundary conditions (18). A free boundary problem has to be solved, since the radius of the plastic zone is unknown.

A quite 'obvious' choice for the fictitious time variable is $\tau = \sigma^0 - p_i$. Note that it would have been possible to take a variable with spatial dimension as the fictitious time one, since its corresponding dimensions would have been absorbed in the plastic multiplier. In this case, the system of partial differential equations (12), (13), (15c) and (16) must be solved with the

boundary conditions (17b) and (18), together with an additional condition on v_r obtained through the matching with the Lamé's solution. In order to compute the ground response curve according to this choice of the fictitious time variable, an initial value problem must be solved.

This problem has a fixed boundary at $r = R$ and a free boundary at $r = R_p$. It should be remarked that the value of the plastic radius for each 'time', i.e. the value of R_p for each p_i, is not known explicitly; rather, the set of conditions imposed at this boundary will determine the location of a point, $r = R_p$, satisfying every condition. This kind of formulation is quite similar to that employed when the ground response curve is obtained through the resolution of a sequence of two-dimensional elasto-plastic boundary value problems with decreasing values of the pressure p_i on the excavation wall. In fact, the only differences between both problems consist in the use of the symmetry to reduce the dimensionality of the problem, and the replacement of the boundary conditions simulating the field stresses 'at infinity' by the boundary conditions at the elasto-plastic interface.

A second choice for the fictitious time variable is $\tau = R_p$. This choice could appear as a less obvious one but, as it will be shown in the next section, it allows reaching a very simple formulation of the problem in order to obtain a certain kind of solutions.

The fact of choosing the radius of the elasto-plastic boundary as the fictitious time variable implies that there is no boundary condition associated to the wall of the tunnel since the internal pressure corresponding to every position of the plastic boundary is *a priori* unknown. At the same time the boundary conditions associated to this elasto-plastic boundary are imposed over a moving free boundary as shown in Equation (18).

4. SOLUTION OF THE PROBLEM BASED ON SELF-SIMILARITY

In order to solve the problem formulated in the previous section, involving the search of radial symmetric solutions, the system of partial differential equations (12), (13), (15c) and (16) has to be solved. The independent variables in these equations are the radial co-ordinate and a fictitious time variable, which has been selected as the radius of the elasto-plastic boundary.

In this section, it will be shown how a family of self-similar solutions of the system of partial differential equations can be obtained. The construction of self-similar solutions relies on the hypothesis that conveniently re-scaled solutions keeps the same form as far as the fictitious time variable evolves, i.e. to say, as far as the size of the plastic zone increases with the unloading of the internal pressure on the tunnel wall [10, 36]. This reduces the system of partial differential equations into a system of ordinary differential equations in terms of the variable associated to the re-scaling. On the other hand, it is also convenient that the solution's re-scaling changes the moving boundary associated to the elasto-plastic interface into a fixed boundary.

The search of self-similar solutions for this equation system stems from the hypothesis that there exist solutions of this kind. Later it will be analysed whether this is true or not, in order to demonstrate that it actually takes place in this way.

Once scaled the radial co-ordinate according to the change of variable $\rho = r/\tau$, and also re-scaled the radial displacements with the plastic radius R_p, the self-similarity hypothesis [37] assumes that the solutions of the radial displacement field and of the stress field do not depend on the plastic radius. This means that the obtained solutions are the stationary ones of the evolution problem in the fictitious time variable. More precisely, it is supposed that a solution, the so-called self-similar solution, of the problem formed by (12), (13), (15c) and (16) exists in

such a way that the functions:

$$\sigma_r(\rho\tau,\tau), \quad \sigma_\theta(\rho\tau,\tau), \quad \frac{1}{\tau}u_r(\rho\tau,\tau) \tag{20}$$

do not depend on the variable τ.

As a whole, it is assumed that as the plastic process evolves, i.e. as the excavation front moves away form the plane of the analysis, and the internal pressure introduced by the convergence–confinement methodology decreases, the strain and stress distributions in the plastic zone keep the same values, when the phenomenon is observed in an appropriate spatial scale.

Taking the above into account, the following functions can be defined:

$$\tilde{u}_r(\rho) = \frac{2G}{\sigma^0 - p_i^*}\frac{1}{\tau}u_r(\rho\tau,\tau) \tag{21}$$

$$\tilde{\sigma}_r(\rho) = \frac{\sigma_r(\rho\tau,\tau)}{\sigma^0 - p_i^*} \tag{22}$$

$$\tilde{\sigma}_\theta(\rho) = \frac{\sigma_\theta(\rho\tau,\tau)}{\sigma^0 - p_i^*} \tag{23}$$

It can be seen that, according to the self-similarity hypothesis, these functions only depend on the re-scaled radial variable ρ. And it can be concluded, as demonstrated in Appendix A, that functions (21)–(23) must be solutions of the system of ordinary differential equations:

$$\begin{bmatrix} 1 & 0 & 0 & 0 \\ 0 & \dfrac{\tilde{B}_4}{2G} & \tilde{B}_2 & \tilde{B}_1 \\ 0 & 0 & 1 & 0 \\ 0 & 1 & -\left(\dfrac{\nu}{\tilde{A}}+1-\nu\right) & \dfrac{1-\nu}{\tilde{A}}+\nu \end{bmatrix} \begin{bmatrix} \dfrac{\mathrm{d}\tilde{u}_r}{\mathrm{d}\rho} \\ \dfrac{\mathrm{d}\tilde{v}_r}{\mathrm{d}\rho} \\ \dfrac{\mathrm{d}\tilde{\sigma}_r}{\mathrm{d}\rho} \\ \dfrac{\mathrm{d}\tilde{\sigma}_\theta}{\mathrm{d}\rho} \end{bmatrix} = \begin{bmatrix} \tilde{v}_r \\ \dfrac{\tilde{B}_3}{2G}\dfrac{1}{\rho^2}\tilde{u}_r - \dfrac{1}{\rho}\tilde{v}_r \\ -\dfrac{\tilde{\sigma}_r}{\rho} + \dfrac{\tilde{\sigma}_\theta}{\rho} \\ -\dfrac{1}{\tilde{A}}\dfrac{1}{\rho^2}\tilde{u}_r + \dfrac{1}{\tilde{A}}\dfrac{1}{\rho}\tilde{v}_r \end{bmatrix} \tag{24}$$

where the first differential equation defines $\tilde{v}_r$, and the coefficients of the equation system appear in Appendix A.

Note that all these coefficients depend on a softening parameter η, and that these coefficients will be frequently given by different formulae in the 'softening' region and the 'residual' one. Remark that the transition between both regimes is detected by the softening parameter. However particular form does the softening parameter take, see Section 2.3, it depends on the 'state' variables σ_r, σ_θ, ε_r, ε_θ, ε_r^p and ε_θ^p. So, in order to solve the described initial value problem, the computation of this parameter must simultaneously be accomplished.

The initial value problem associated with this system of ordinary differential equations has to be solved according to the initial conditions imposed by the Lamé's solution in the elastic–plastic interface. These initial conditions are actually final conditions due to the fact that the problem must be solved for values of ρ in an interval $[\rho_{inf}, 1]$, corresponding to the plastic zone—given in physical co-ordinates by $[R<r<R_p]$—where ρ_{inf} is unknown at this stage (see below how to stop the integration of the initial value problem in order to complete the

computation of the ground response curve):

$$\begin{aligned} \tilde{\sigma}_r(1) &= \tilde{\sigma}^0 - 1 \\ \tilde{\sigma}_\theta(1) &= \tilde{\sigma}^0 + 1 \\ \tilde{u}_r(1) &= 1 \\ \frac{\mathrm{d}\tilde{u}_r}{\mathrm{d}\rho}(1) &= \tilde{v}_r(1) = -1 \end{aligned} \tag{25}$$

The regularity of the coefficient matrix of this differential equation system and thus, the solvability of the initial value problem is ensured whenever the selected failure criterion and plastic potential fulfill the following condition, see Section 2.2:

$$H_0 + H_t > 0 \tag{26}$$

For very small values of this addition, the solutions of the initial value problem contain a narrow boundary layer around the initial condition. This condition is associated to the rapid transition from the elastic regime—corresponding to the initial condition—to the residual regime, through the softening zone. In the extreme case, represented by the condition $H_0 + H_t = 0$, an elastic-brittle material is represented, where a discontinuity in the displacement derivative—associated to the strain discontinuity—takes place [10].

Hence, once condition (26) is satisfied—for failure criteria and flow rules described by regular functions, the existence of solutions for the initial value problem associated to the construction of self-similar solutions is assured. Nevertheless, the uniqueness of the solution is not guaranteed for 2D boundary value problems associated with strain calculations around excavations in materials, which exhibit softening or non-associated flow rules; since, for this kind of materials, uniqueness sufficient conditions are not met [38, 32]. It is then possible for the sequence of boundary value problems to present bifurcation phenomena within the unloading process. In this case, there will appear additional solutions of the 2D boundary value problem lacking radial symmetry. At the same time, neither can localization phenomena be excluded in the bifurcated solutions.

In such cases, the self-similar solution here presented corresponds to the fundamental 'branch' of solutions, starting from which, bifurcation may take place producing non-symmetric solutions of the two-dimensional problem. Remark that if the boundary value problem has a unique solution, this solution must be radial-symmetric. With the loss of uniqueness, the radial-symmetric solution will also lose stability, which will be transferred to the bifurcated solutions (in practice, the existence of imperfections will select just one of these solutions). This implies that, after bifurcation takes place, the physically observed solution will no longer be the symmetric one.

Against this background, self-similar solutions are interesting in two ways. First, as they correspond to the fundamental 'branch' of solutions, the critical load pressure, i.e. the internal pressure for which bifurcation takes place, can be computed using self-similar solutions. Secondly, which is more important from the practical point of view, displacement values given by the ground response curve computed for self-similar solutions seem to agree quite well with mean values obtained for the bifurcated solutions in the 2D boundary value problem [39]. In this way, self-similar solutions provide the most significant information searched by the convergence–confinement methodology in order to compute ground response curves.

Starting from the solution of the initial value problem, the complete solution of the ground reaction curve or convergence–confinement curve—the radial displacement values in the excavation boundary related to every value of internal pressure—can be easily obtained. Certainly, for every value of ρ smaller than unity, the pair of values $[\tilde{u}_r(\rho), \tilde{\sigma}_r(\rho)]$ corresponds to one point in the ground reaction curve. This is due to the fact that the value $\tilde{u}_r(\rho)$ gives the radial displacement in the tunnel wall for an internal pressure given by the value $\tilde{\sigma}_r(\rho)$. Hence, in practice, in order to obtain the full ground reaction curve, it suffices with calculating the described initial value problem from $\rho = 1$, until the value of ρ, which makes the radial stress null.

The derived initial value problem does not generally have an analytical solution—except for very simple cases such as that of the Tresca failure criterion, for which the presented equations become much simpler [10], so it should be solved by means of numerical integration. In what follows, the integration process is carried out according to the Runge–Kutta–Fehlberg method proposed by Dormand and Price [40]. This technique combines methods of fourth- and fifth-order for the integration step adaptation and it is programmed in the MATLAB environment under the function named 'ode45'. The fact of working in this environment makes it easier to run multiple parameter problems. It also facilitates the presentation of data.

At this stage it should be emphasized the remarkable difference on the computational cost between the alternative presented to obtain the ground reaction curve—integration of one initial value problem—and the other one of solving a set of two-dimensional problems. In general terms, the time needed to solve the problem according to the presented methodology is just a few seconds, whereas the time needed to solve the same case by means of FDM-based code FLAC-2D varies from some minutes to few hours depending on the level of mesh refinement. In Section 5.1.2, the exact computational cost corresponding to a particular case is provided.

5. ANALYSIS OF SOME EXAMPLES

5.1. Self-similar solution for Mohr–Coulomb criteria and simple hypothesis

In order to obtain the self-similar solution, a system of ordinary differential equations has been derived supposing: (i) yield criterion, (ii) plastic potential, (iii) piecewise linear functions of materials and (iv) plastic parameter. A special case is presented with the following conditions:

(i) *Mohr–Coulomb yield criterion*:

$$f(\sigma_\theta, \sigma_r, \eta) = \sigma_\theta - K_p(\eta)\sigma_r - 2C(\eta)\sqrt{K_p(\eta)} \tag{27}$$

(ii) *Plastic potential*:

$$g(\sigma_\theta, \sigma_r, \eta) = \sigma_\theta - K(\eta)\sigma_r \tag{28}$$

where $K(\eta)$ is known as the dilation coefficient, having the same form as the passive reaction coefficient, but replacing the friction function by the dilation one:

$$K(\eta) = \frac{1 + \sin\psi(\eta)}{1 - \sin\psi(\eta)} \tag{29}$$

(iii) Two-segment piecewise linear functions of plastic parameter for cohesion $C(\eta)$, friction $\phi(\eta)$ and dilation $\psi(\eta)$ being, ϕ^p, C^p and ψ^p the peak parameters and ϕ^r, C^r and ψ^r the residual

ones [41]. The elastic regime is characterized by shear modulus G and Poisson's ratio v. The plastic one is characterized by friction, cohesion and dilation functions as follows:

$$\phi(\eta) = \begin{cases} \phi^{\mathrm{p}} - \dfrac{\phi^{\mathrm{p}} - \phi^{\mathrm{r}}}{\eta^*}\eta, & 0 < \eta < \eta^* \\ \phi^{\mathrm{r}}, & \eta \geqslant \eta^* \end{cases}$$

$$C(\eta) = \begin{cases} C^{\mathrm{p}} - \dfrac{C^{\mathrm{p}} - C^{\mathrm{r}}}{\eta^*}\eta, & 0 < \eta < \eta^* \\ C^{\mathrm{r}}, & \eta \geqslant \eta^* \end{cases} \tag{30}$$

$$\psi(\eta) = \begin{cases} \psi^{\mathrm{p}} - \dfrac{\psi^{\mathrm{p}} - \psi^{\mathrm{r}}}{\eta^*}\eta, & 0 < \eta < \eta^* \\ \psi^{\mathrm{r}}, & \eta \geqslant \eta^* \end{cases}$$

(iv) *The plastic parameter used is the plastic shear strain*:

$$\eta = \gamma^{\mathrm{p}} = \varepsilon_\theta^{\mathrm{p}} - \varepsilon_r^{\mathrm{p}} \tag{31}$$

Taking into account that plastic strains can be obtained from total and elastic strains, the variable changes proposed and the self-similar hypothesis, an expression for the plastic parameter can be obtained in self-similar form as follows:

$$\tilde{\eta}(p) = \frac{\sigma^0 - p_{\mathrm{i}}^*}{2G}\frac{\tilde{u}_r(\rho)}{\rho} - \frac{\sigma^0 - p_{\mathrm{i}}^*}{2G}\frac{\mathrm{d}\tilde{u}_r(\rho)}{\mathrm{d}\rho} - \frac{\sigma^0 - p_{\mathrm{i}}^*}{2G}\tilde{\sigma}_\theta(\rho) + \frac{\sigma^0 - p_{\mathrm{i}}^*}{2G}\tilde{\sigma}_r(\rho) \tag{32}$$

Once defined all these functions, the corresponding coefficients of the system of differential ordinary equations are obtained and presented in Appendix B.

The system of equations can be written in matrix form as follows:

$$M(\rho, \bar{y})\frac{\mathrm{d}\bar{y}}{\mathrm{d}\rho} = \bar{\Phi}(\rho, \bar{y}) \tag{33}$$

where M is the matrix of the coefficients of the system of equations whose resolution will yield vector $y = (\tilde{u}_r(\rho), \tilde{v}_r(\rho), \tilde{\sigma}_\theta(\rho), \tilde{\sigma}_r(\rho))$, which includes radial displacements, displacement velocities and hoop and radial stresses around the excavation.

5.1.1. Tresca failure criterion. As shown in Table I, the only analytical solution concerning strain-softening behaviour is obtained supposing Tresca yield criterion [10], so a comparison between both self-similar and analytical solutions has been made. In Figures 6 and 7, the ground reaction curves and evolution of plastic radii (softening and residual ones) with internal pressure are shown for both solutions. As it can be observed the self-similar solution accurately recuperates the analytical one [10]. In these figures, R_{p} and R_{p}^* represent the extent of the softening and residual plastic zones, respectively.

The elasto-plastic softening behaviour with Tresca yield criterion is a specific case, since some terms of the coefficients of the system of equations are null. Then it would be more appropriate to compare a self-similar solution with the numerical solution by means of code FLAC-2D [31] for a more general case (Mohr–Coulomb yield criterion).

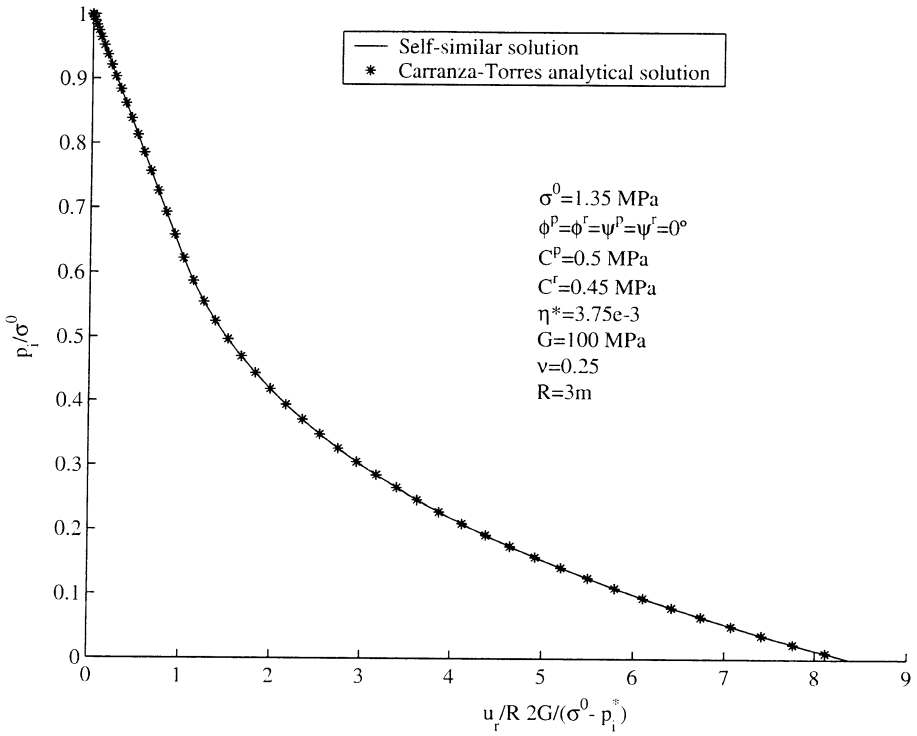

Figure 6. Ground reaction curve. Strain-softening behaviour and Tresca yield criterion.

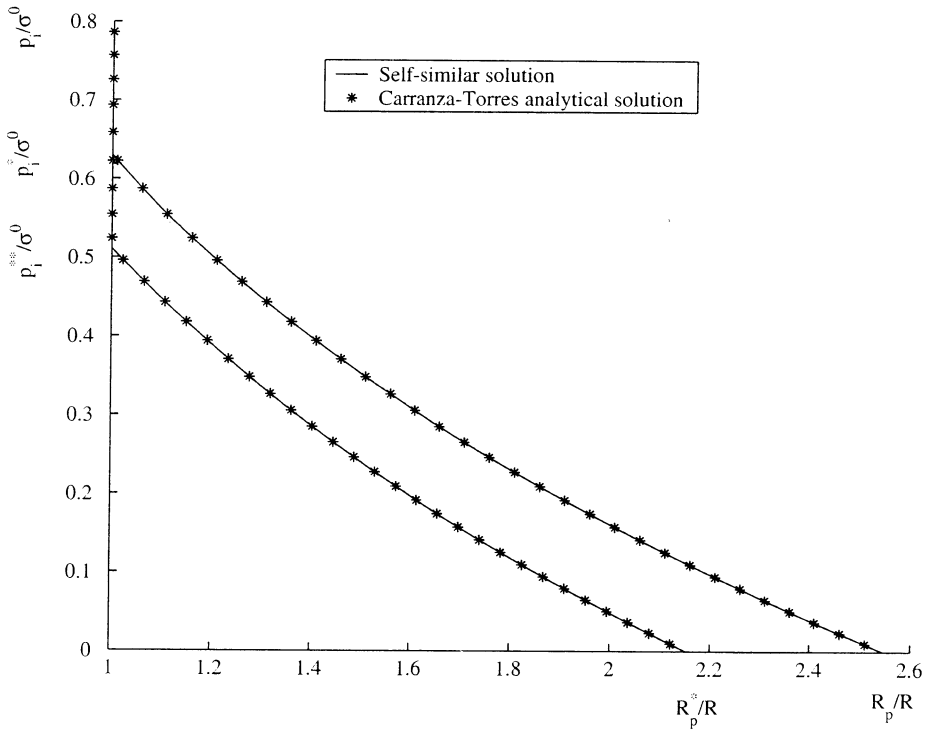

Figure 7. Evolution of plastic radii with internal pressure. Strain-softening behaviour and Tresca yield criterion.

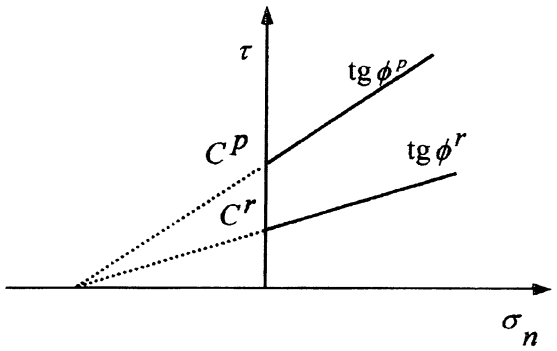

Figure 8. Obtaining residual values for the Mohr–Coulomb criterion using β model.

5.1.2. Mohr–Coulomb failure criterion. In order to reduce the number of variables a new parameter β is defined, in such a way that for a Mohr–Coulomb failure criterion, the residual parameters can be obtained starting from the peak ones as follows:

$$C^{\mathrm{r}} = (1 - \beta)C^{\mathrm{p}}, \quad \mathrm{tg}\,\phi^{\mathrm{r}} = (1 - \beta)\,\mathrm{tg}\,\phi^{\mathrm{p}} \tag{34}$$

This allows eliminating a material parameter and it seems a reasonable proposition from analysis of References [11, 23, 42, 43]. See Figure 8.

The parameter β, which will be referred to as the *strength loss* parameter, quantifies the jump of strength from the peak or intact condition to the residual condition [44]. 'β' falls by definition within 0 and 1. If it is 0 it implies no loss of strength, so the perfectly plastic behaviour model is retrieved, whereas if it is 1, the material losses all its strength after failure. The use of this β parameter is based on the assumption that after the peak strength of the material is exceeded, the material losses cohesive and frictional strength in similar proportion. This approach, which does not necessarily suits all rock masses, is done in order to simplify the outputs of the presented examples.

Figures 9 and 10 show a comparison between the self-similar solution and numerical two-dimensional solution by means of FLAC-2D [31]. As it can be seen, the self-similar solution adjusts to the numerical one, although some differences can be appreciated, never being larger than 10%. It has to be taken into account that two numerical solutions are being compared: the first one is one-dimensional, and the second one two-dimensional. The reason for the differences observed is probably due to the spatial discretization made by code FLAC-2D. The plastic parameters used in the simulations are equivalent, because in case of constant dilation, as shown previously in Section 2.4, there is a relation between FLAC-2D plastic parameter and the principal plastic strains difference used to build the self-similar solution.

In order to remark the differences on the computational cost between both methods, the time needed to perform the corresponding calculations for this Mohr–Coulomb case by means of a Pentium III (128 MB RAM) computer was measured. Having done so, the time required to solve the self-similar problem in MATLAB 6.0 was 4.07 s. The time required for obtaining the complete ground reaction curve with code FLAC-2D with a 900-zone mesh was 7 min and 54 s, whereas with a 3600-zone mesh was 148 min. In this last case bifurcation was observed.

5.1.2.1. Parametric analysis. As it has been observed, the proposed methodology obtains the ground reaction curve, which can be also calculated by means of standard FDM or FEM-based

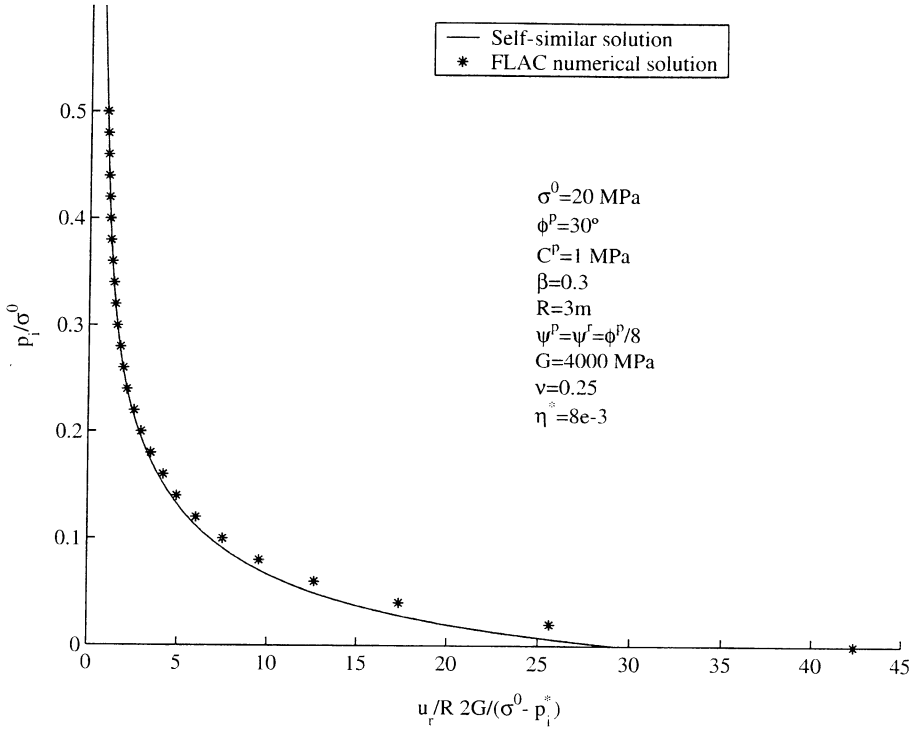

Figure 9. Ground reaction curve. Self-similar and FLACs comparison solution. Strain-softening behaviour and Mohr–Coulomb yield criterion.

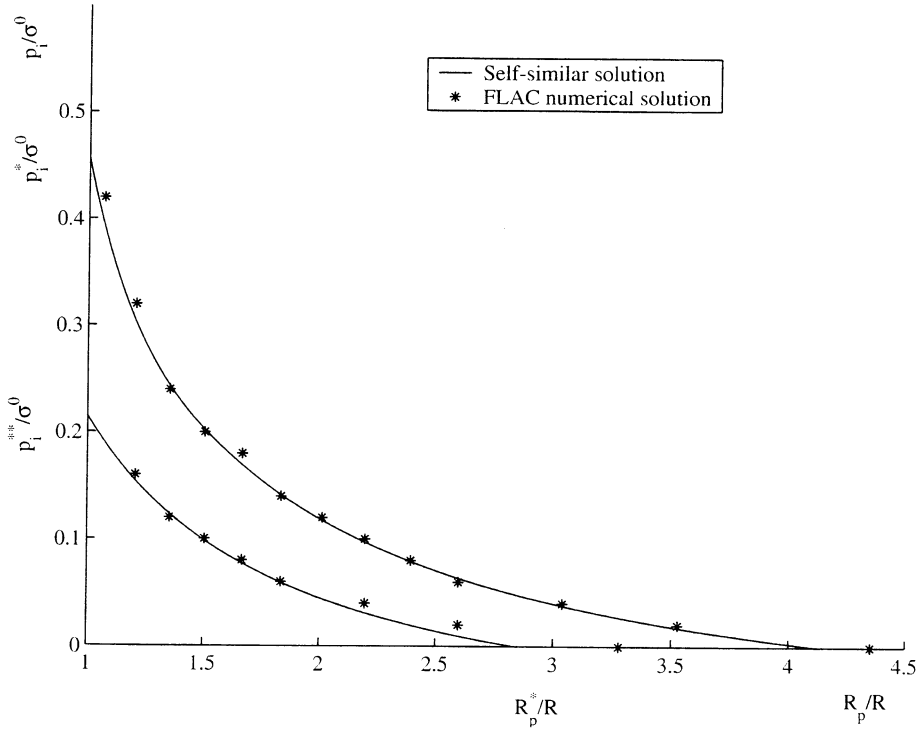

Figure 10. Evolution of plastic radii. Self-similar and FLACs comparison solution. Strain-softening behaviour and Mohr–Coulomb yield criterion.

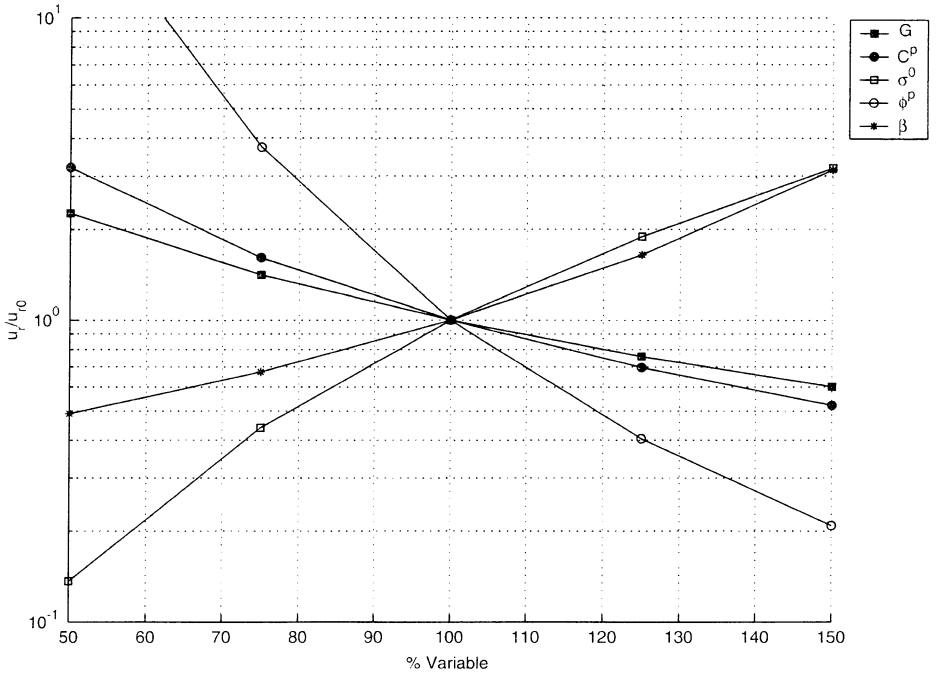

Figure 11. Influence of most significant parameters in final radial displacement. Strain-softening behaviour and Mohr–Coulomb yield criterion.

codes. One of its main advantages is that it does so more efficiently than these codes, which permits performing parametric studies more rapidly. Parametric studies are usually very recommendable in a discipline like geomechanics where a certain deal of uncertainty is always expected. This kind of analysis is very helpful in order to conveniently control uncertainty throughout the design and construction process.

As an illustrative example, a parametric study of a tunnel excavated in an average quality rock mass is performed in what follows. A 3 m radius tunnel is drilled in a softening material—subject to an isotropic stress field of $\sigma^0 = 20$ MPa—with elastic parameters $G = 4000$ MPa and $\nu = 0.25$. Peak cohesion is 1 MPa and peak friction is 30°, whereas the strength loss parameter β equals 0.3. The peak dilation angle is 10° while the residual one is 5°. The value of the softening parameter that indicates the transition to the residual regime is chosen to be $\eta^* = 0.008$.

The model is run in MATLAB and a subroutine is programmed to vary every single input parameter from 50 to 150% of its initial value in such a way that spider diagrams—relating any output parameter with the different varying values of every input parameter—can be easily obtained. As an example, Figure 11 illustrate the parametric study concerning the final displacement value on the tunnel wall, showing the relative significance of the most significant input data on this final output. For this particular case, the strength loss parameter and the peak failure criterion input values seem to control the final displacements results. Gumusoglu *et al.* [24] report analogous results in a similar analysis performed by means of a FEM-based code.

According to the presented method not only the final displacement value, computed in the spider diagram, can be easily analysed, but also the full GRC corresponding to different values of the different input parameters. In this way, Figures 12–15 show different GRC obtained by varying the most significant parameters. These results, which can be very useful from a practical

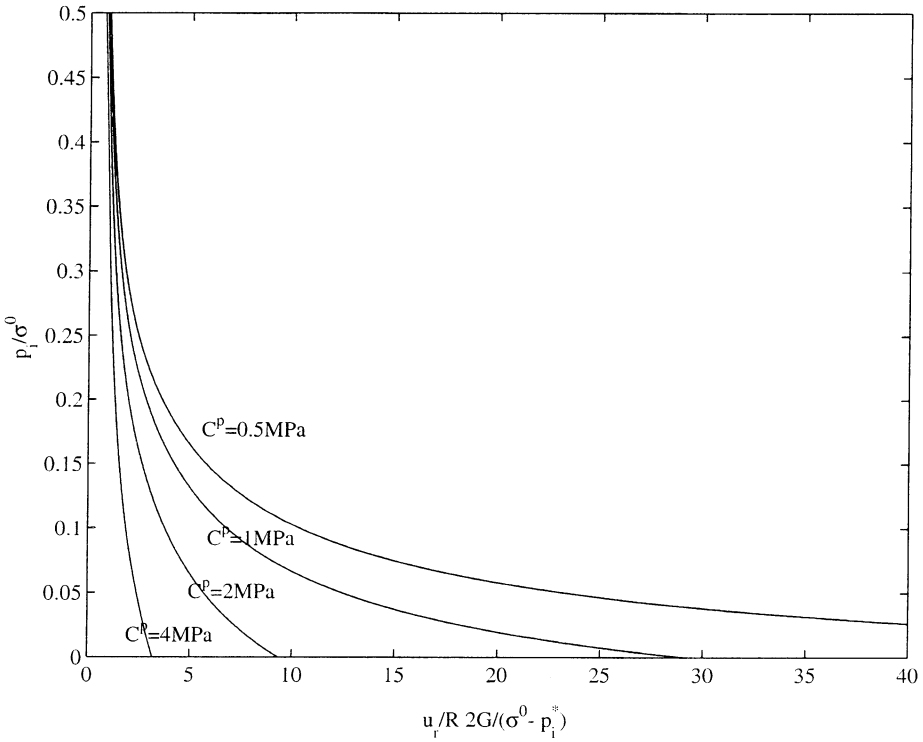

Figure 12. Influence of peak cohesion in GRC. Strain-softening behaviour and Mohr–Coulomb yield criterion.

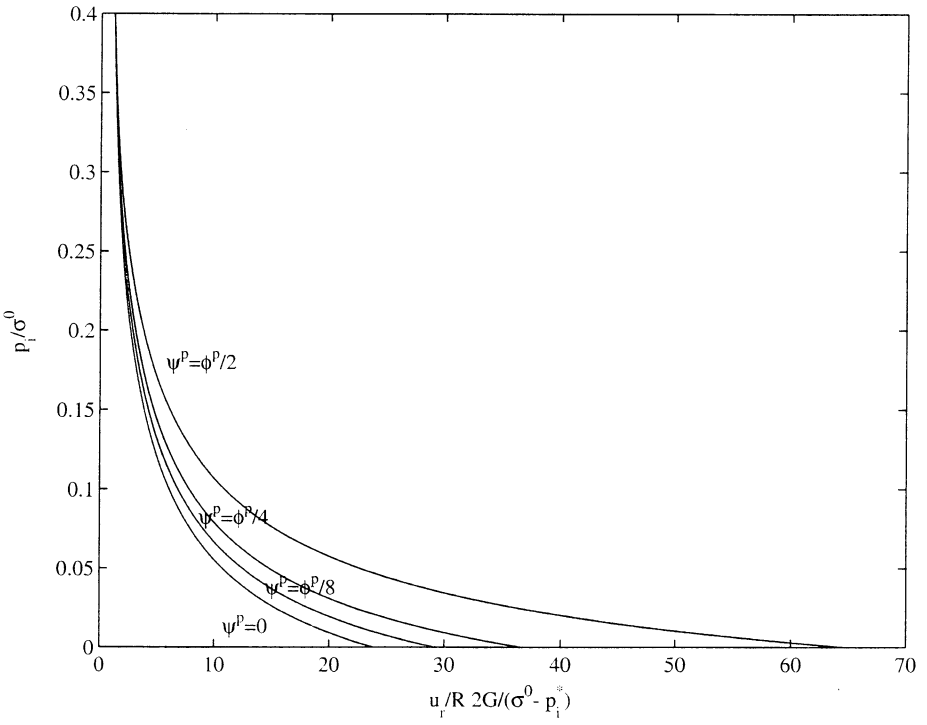

Figure 13. Influence of peak dilation angle in GRC. Strain-softening behaviour and Mohr–Coulomb yield criterion.

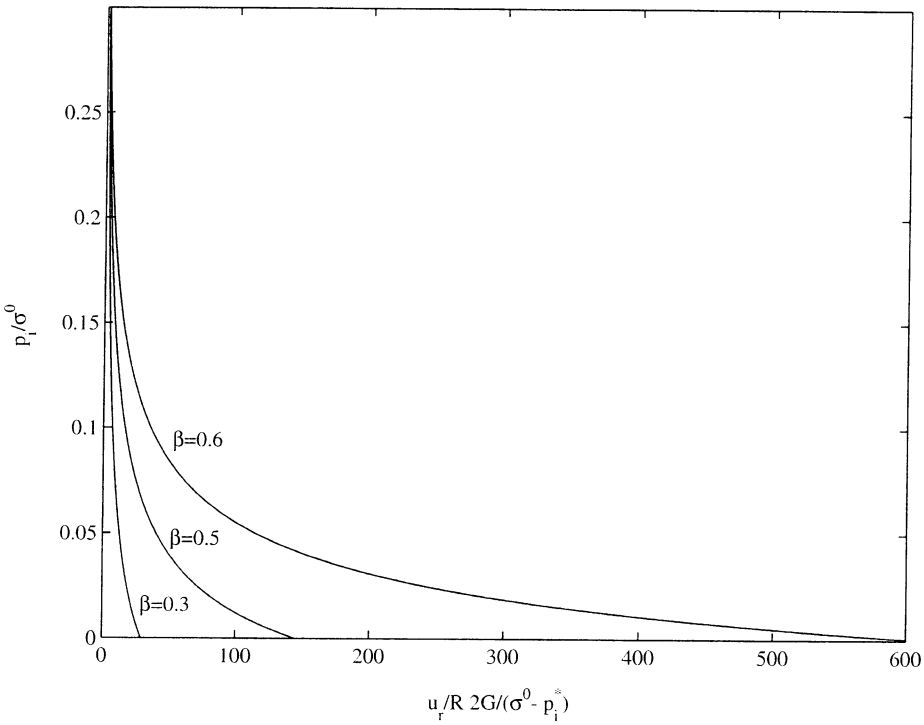

Figure 14. Influence of β parameter in GRC. Strain-softening behaviour and Mohr–Coulomb yield criterion.

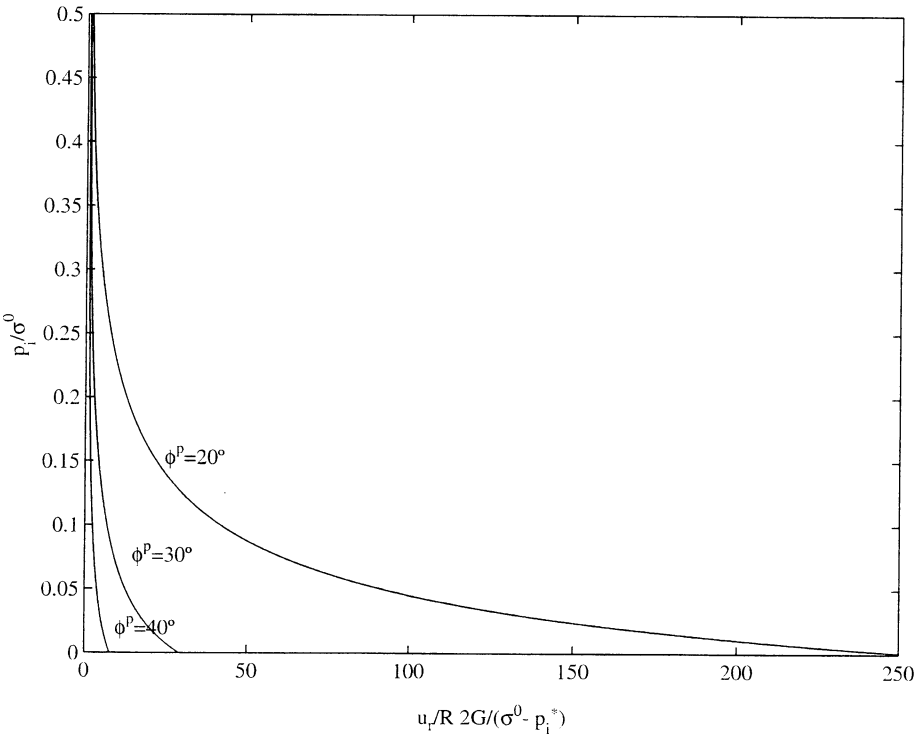

Figure 15. Influence of peak friction angle in GRC. Strain-softening behaviour and Mohr–Coulomb yield criterion.

design scope, are obtained with MATLAB in a fast and easy way, whereas to obtain the same information by means of a standard numerical code, i.e. FLAC-2D, would have taken much longer.

5.1.2.2. Graphic representation considering strain-softening behaviour and Mohr–Coulomb yield criterion. A self-similar solution has been obtained for the case of strain-softening behaviour solving a system of ordinary differential equations. It is useful to obtain a simple chart, which is able to represent a determined range of rock masses under a range of far-field stresses [10]. The self-similar solution gives values of radial displacement, hoop and radial stresses and softening and residual plastic radii as functions of the variable ρ. Thus, taking advantage of the efficiency of the method, the main results for varying input parameters can be plotted in a compact form.

The number of parameters controlling the tunnel behaviour—once reduced the number of variables by means of the corresponding simplifications—are seven: Poisson's ratio ν, peak friction ϕ^p, peak cohesion C^p, β, field stress σ^o, dilation (also considered constant $\psi^p = \psi^r$) and η^*. The shear modulus G and the radius of the excavation R are normalized. In order to plot the ground reaction curve, only two parameters can be varied, leaving the other five constant. In order to build the charts, peak cohesion, peak friction, dilation, β and the Poisson's ratio have been left constant and far field stress and η^* are assigned a wide range of values.

In what concerns the far-field stress, an initial value of 0.5 times the unconfined strength of the rock mass and a final value of 10 times the unconfined strength of the rock mass have been considered. When the far field stress is too high, an upper limit of 30 MPa is considered.

As an example, charts for rock masses with $C^p = 1$ MPa, $\phi = 30°$, $\beta = 0.5$, $\psi^p = \psi^r = 3.75°$ and $\nu = 0.25$ are presented in Figures 16–19.

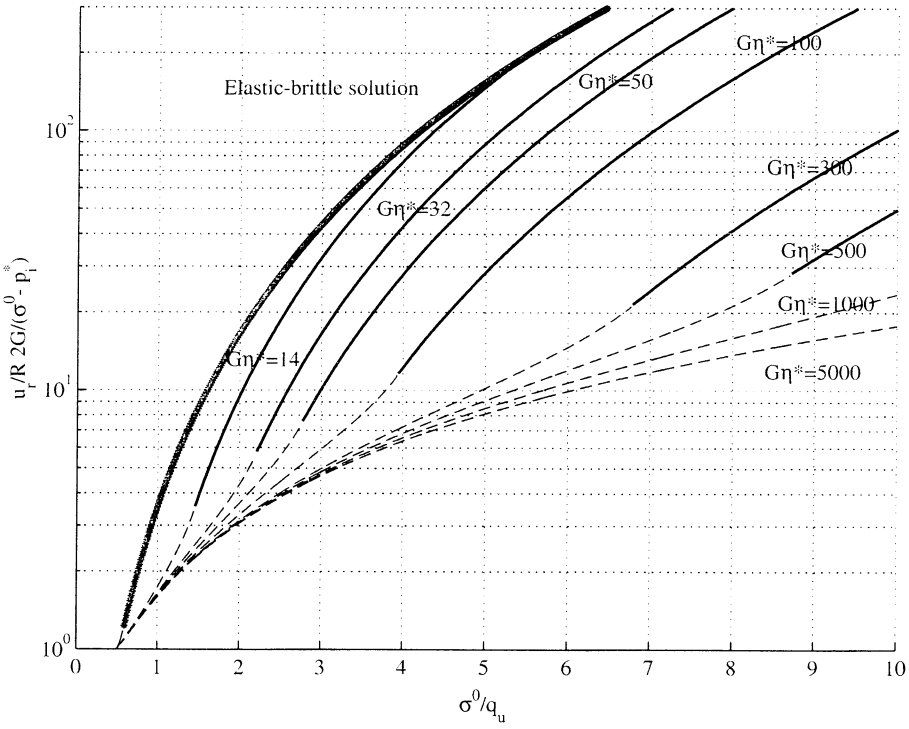

Figure 16. Final radial displacement. Strain-softening behaviour and Mohr–Coulomb yield criterion. $\phi^p = 30°$, $\psi^p = \psi^r = \phi^p/8$, $C^p = 1$ MPa, $\nu = 0.25$, $\beta = 0.3$.

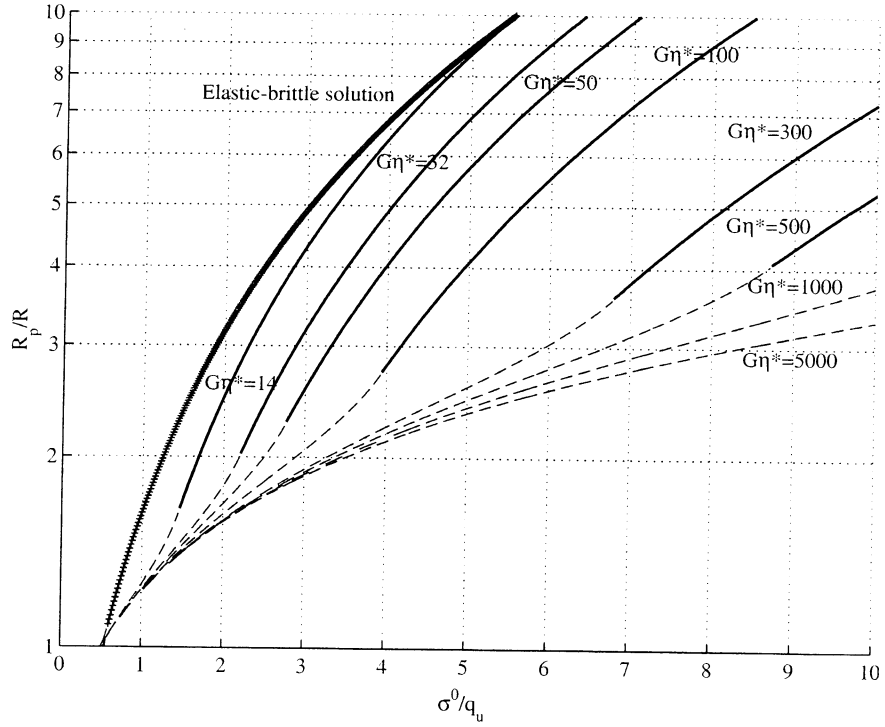

Figure 17. Final softening plastic radius. Strain-softening behaviour and Mohr–Coulomb yield criterion. $\phi^p = 30°$, $\psi^p = \psi^r = \phi^p/8$, $C^p = 1$ MPa, $\nu = 0.25$, $\beta = 0.3$.

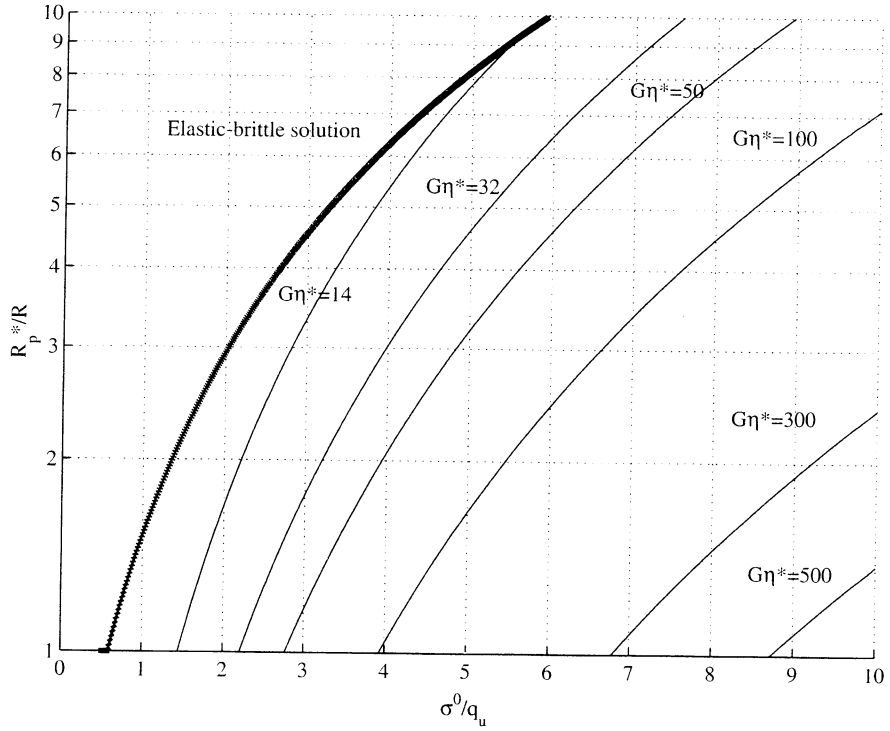

Figure 18. Final residual plastic radius. Strain-softening behaviour and Mohr–Coulomb yield criterion. $\phi^p = 30°$, $\psi^p = \psi^r = \phi^p/8$, $C^p = 1$ MPa, $\nu = 0.25$, $\beta = 0.3$.

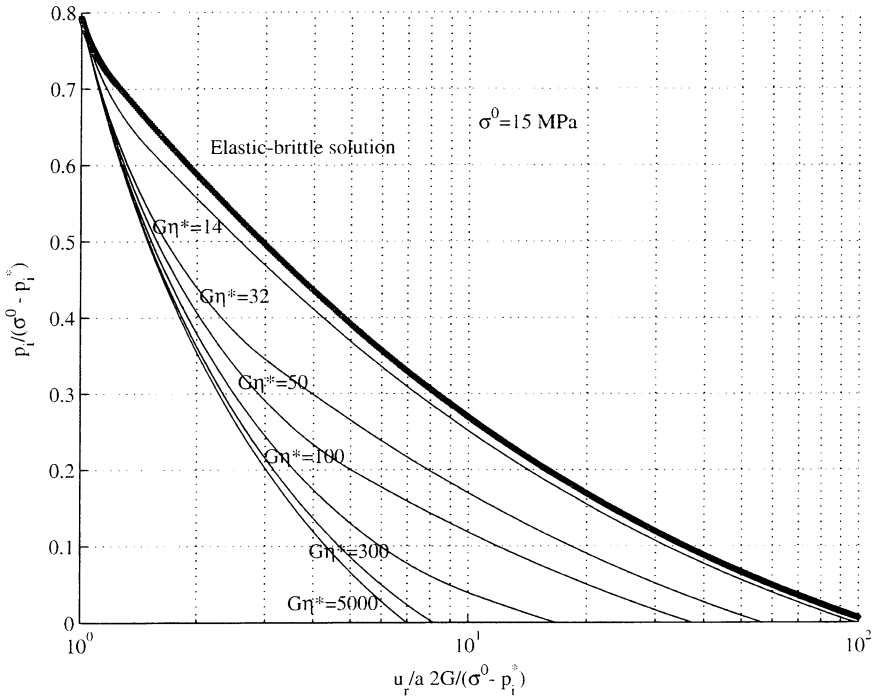

Figure 19. Ground reaction curves for $\sigma^0 = 15$ MPa. Strain-softening behaviour and Mohr–Coulomb yield criterion. $\phi^p = 30°$, $\psi^p = \psi^r = \phi^p/8$, $C^p = 1$ MPa, $\nu = 0.25$, $\beta = 0.3$.

In Figure 16 the final radial displacement is presented (being q_u the peak rock mass strength) for different values of field stress and $G\eta^*$. Also the elastic brittle [10] solution is presented, and it can be considered as a limit of the elasto-plastic softening behaviour. The solution for perfect elasto-plastic behaviour would be found for very high values of $G\eta^*$.

This kind of charts (Figure 16) has the advantage that they also indicate the final state of the excavation wall. In this way, if the final displacement lies in a dashed line, it indicates that only the softening state has developed, whereas if in a solid line, the residual state has been reached.

In Figure 17, the plastic softening radius is presented for different values of $G\eta^* = \text{const}$. The same considerations concerning the achievement of the residual state as indicated above stands for this graph. The residual plastic radius is illustrated in the third chart (Figure 18).

These charts can be used to obtain information about final radial displacement and plastic radii. In most cases and when applying the convergence–confinement methodology, the complete ground-reaction curve is needed. In Figure 19 the ground reaction curves for a specific far-field stress and a range of values of $G\eta^* = \text{const.}$ are presented.

Complementarily, Alonso [36] presents the charts for 16 average quality rock masses, including final radial displacement and final plastic radii charts, together with the complete GRC for different far-field stress. These charts, which can be rapidly obtained, could be of much help for the tunnel designer.

5.2. Self-similar solution for Hoek–Brown criterion and simple hypothesis

Since the Hoek–Brown failure criterion is widely popular within the geomechanics community, it has also been implemented within the framework of the general methodology shown here.

In this case, being the material parameters $m(\eta)$, $s(\eta)$ and the intact compressive strength σ_{ci}, the failure criterion is given by

$$f(\sigma_\theta, \sigma_r, \eta) = \sigma_\theta - \sigma_r - \sqrt{m(\eta)\sigma_r\sigma_{ci} + s(\eta)\sigma_{ci}^2} \tag{35}$$

The Mohr–Coulomb form of the plastic potential is maintained:

$$g(\sigma_\theta, \sigma_r, \eta) = \sigma_\theta - K(\eta)\sigma_r \tag{36}$$

The plastic parameter is $\eta = \gamma^p = \varepsilon_\theta^p - \varepsilon_r^p$ and also piecewise linear functions are considered, where m^p and s^p are the peak values, and m^r and s^r the residual ones.

$$\begin{aligned} m(\eta) &= \begin{cases} m^p - \dfrac{m^p - m^r}{\eta^*}\eta, & 0 < \eta < \eta^* \\ m^r, & \eta \geqslant \eta^* \end{cases} \\ s(\eta) &= \begin{cases} s^p - \dfrac{s^p - s^r}{\eta^*}\eta, & 0 < \eta < \eta^* \\ s^r, & \eta \geqslant \eta^* \end{cases} \end{aligned} \tag{37}$$

The coefficients of the system of ordinary differential equations are shown in Appendix C. In Figures 20 and 21, ground reaction curves and evolution of plastic radii are shown.

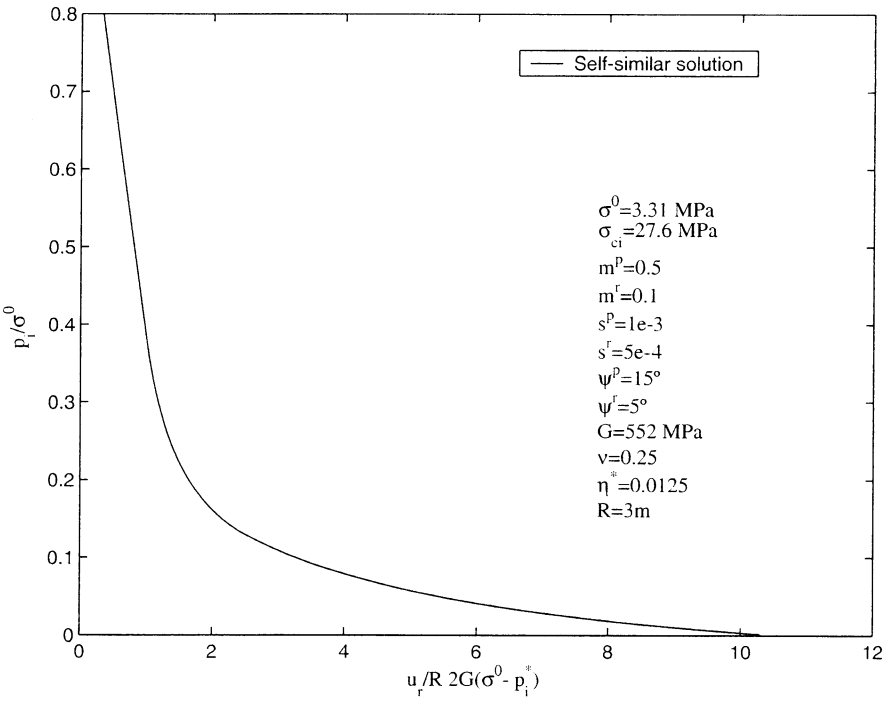

Figure 20. Ground reaction curve. Strain-softening behaviour and Hoek–Brown yield criterion.

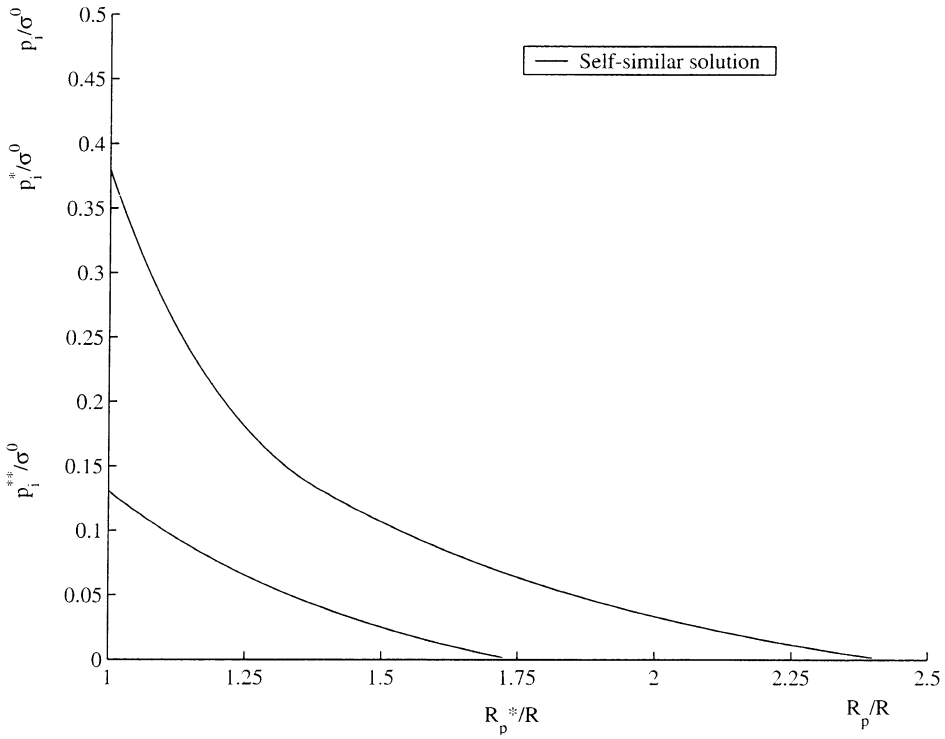

Figure 21. Plastic radii of softening and residual zones. Strain-softening behaviour and Hoek–Brown yield criterion.

6. CONCLUSIONS

The so-called 'convergence–confinement' method of interpreting the interaction between ground and support in tunnels has proved to be a useful tool and has notably contributed to gain insight into the preliminary support design. Nevertheless, it should always be used within a wider and more general frame of design and construction 'design as you go' philosophy, based on the rapid decision-making according to the in-place ground control measurements taken. To be able to obtain more realistic ground reaction curves contributes on one hand to a better knowledge of the rock masses in the underground works, and on the other hand to design more accurately the appropriate support or reinforcement.

There exist closed-form solutions for obtaining the ground reaction curves for most cases concerning perfectly plastic and perfectly brittle materials, but it seems that there are not enough general solutions in literature concerning strain-softening materials, which even if somewhat controversial, is a type of behaviour significant and commonly observed in rock masses. Even if it is possible to obtain GRC for tunnels excavated in strain-softening materials by means of standard FEM or FDM based codes [24, 45], this process tends to be very time-consuming. This makes very difficult performing parametric analyses and then, much of the enriching generality inherent to the 'convergence–confinement' method is lost.

In order to be able to obtain more efficiently the GRC of circular tunnels excavated in rock masses exhibiting strain-softening behaviour and subject to isotropic stress fields, a system of ordinary differential equations has been developed. This system of equations is derived from the usual partial differential equations system for the radial symmetric solutions through a

self-similarity hypothesis. A change of variable has allowed transforming the boundary value problem into an initial value one. This formulation approach has permitted the retrieval of the solution to the problem in a much easier and efficient way than the two-dimensional numerical solution of the problem. This has a clear advantage over the two-dimensional numerical techniques. The final initial boundary problem can be simply numerically solved in order to obtain the GRC for generic materials in what concerns (i) failure criterion, (ii) plastic potential or flow rule, (iii) softening parameter and (iv) piecewise material functions. The plastic parameter is defined to be a function of the principal plastic strains.

The solution methodology has been implemented for some common cases in MATLAB environment by means of an in-built subroutine, permitting on the one hand to obtain more rigorous solutions for strain-softening materials, but also to have a more widely usable tool to implement different or less-common material models. For instance, it is now being used to implement a model with confinement stress-dependent dilation, which seems to agree well with some in situ observations. It is also being used to perform studies on bifurcation and localisation phenomena in tunnels, since the method can track the so-called fundamental branch of solutions.

In order to show different practical applications of the general methodology, some illustrative examples have been presented. Firstly, an example of Tresca—frictionless Mohr–Coulomb—failure criterion with non-associated flow rule is performed and the results agree well with those obtained using a rigorous closed-form solution [10].

Then, an example of Mohr–Coulomb failure criterion with non-associated flow rule and piecewise linear functions of intact failure parameters and dilation angle has been solved. In order to simplify the interpretation of results the so-called β-model [10] has been used. Results compare well with those obtained by means of a finite difference method based 2D numerical code [31]. To take advantage of one of the strongest points of the method—short calculation time—a parametric study has been performed in order to highlight the significance of the different parameters on the results. The peak or intact strength parameters, together with the so-called strength drop or 'β' seem to be the most significant for the case analysed. In order to quantify the influence of the 'drop modulus' on results, four types of charts have been developed, where the final displacement in the tunnel wall, the radii of the softening and residual zone and the ground reaction curve with changing values of σ^0, and $G\eta^*$ are obtained. These charts are a good basis to show how the perfectly brittle and perfectly plastic behaviour models are but limiting cases of the most general strain-softening behaviour model. The Hoek–Brown failure criterion has also been implemented and an example is presented.

The proposed solution methodology for obtaining the ground reaction curve for tunnels excavated in materials exhibiting strain-softening provides a general framework to solve these problems in a more efficient and less time consuming way than with standard 2D numerical methods. It also permits incorporating new features in this behaviour model, such as dependencies between parameters, which make this method especially suited to perform further analyses.

ACKNOWLEDGEMENTS

The authors thank the local government of Galicia (Xunta de Galicia), Spain, for financial support of the research project entitled 'Elasto-plastic analysis of tunnels excavated in strain-softening rock masses', under contract reference number (PGIDT00PXI32101PR).

APPENDIX A: SYSTEM OF ORDINARY DIFFERENTIAL EQUATIONS ACCORDING TO THE SELF-SIMILARITY HYPOTHESIS

This appendix presents the derivation of the system of ordinary differential equations obtained starting from equilibrium (12), persistence—or active plasticity—(13), radial displacement velocity (15c) and flow rule (3) equations, when the self-similarity hypothesis is considered.

If this self-similarity condition:

$$\frac{\partial}{\partial\tau}(u_r(\rho\tau,\tau)) = \frac{\partial}{\partial\tau}(\sigma_r(\rho\tau,\tau)) = \frac{\partial}{\partial\tau}(\sigma_\theta(\rho\tau,\tau)) = 0 \tag{A1}$$

is considered, then, the following relations can be obtained by differentiating equations (21), (22) and (23):

$$\begin{aligned}
\frac{\mathrm{d}\tilde{u}_r(\rho)}{\mathrm{d}\rho} &= \frac{2G}{\sigma_0 - p_i^*}\frac{\partial u_r(\rho\tau,\tau)}{\partial r}\\
\frac{\mathrm{d}\tilde{u}_r^2(\rho)}{\mathrm{d}\rho} &= \frac{2G}{\sigma_0 - p_i^*}\tau\frac{\partial^2 u_r(\rho\tau,\tau)}{\partial r^2}\\
\frac{\mathrm{d}\tilde{\sigma}_r(\rho)}{\mathrm{d}\rho} &= \frac{1}{\sigma_0 - p_i^*}\tau\frac{\partial\sigma_r(\rho\tau,\tau)}{\partial r}\\
\frac{\mathrm{d}\tilde{\sigma}_\theta(\rho)}{\mathrm{d}\rho} &= \frac{1}{\sigma_0 - p_i^*}\tau\frac{\partial\sigma_\theta(\rho\tau,\tau)}{\partial r}
\end{aligned} \tag{A2}$$

In what follows and for sake of simplicity, the explicit dependence on ρ, is not provided whenever there is no possible ambiguity.

In the sequel, the so-called equilibrium equation (12) becomes:

$$\frac{\mathrm{d}\tilde{\sigma}_r}{\mathrm{d}\rho} = -\frac{\tilde{\sigma}_r - \tilde{\sigma}_\theta}{\rho} \tag{A3}$$

Starting from (4), (15a) and (15b), taking into account that total strain can be subdivided into the corresponding elastic and plastic parts and introducing the classic expression for the elastic strain it is possible to conclude:

$$\begin{aligned}
\dot{\varepsilon}_r^{\mathrm{p}}(\rho\tau) &= \frac{r}{\tau^2}\frac{\sigma_0 - p_i^*}{2G}\left[-\frac{\mathrm{d}^2\tilde{u}_r}{\mathrm{d}\rho^2}(\rho) + (1-\nu)\frac{\mathrm{d}\tilde{\sigma}_r}{\mathrm{d}\rho}(\rho) - \nu\frac{\mathrm{d}\tilde{\sigma}_\theta}{\mathrm{d}\rho}(\rho)\right]\\
\dot{\varepsilon}_\theta^{\mathrm{p}}(r,\tau) &= \frac{\sigma_0 - p_i^*}{2G}\left[-\frac{1}{\tau}\frac{\mathrm{d}\tilde{u}_r}{\mathrm{d}\rho}(\rho) + \frac{1}{r}u_r(\rho) + (1-\nu)\frac{r}{\tau^2}\frac{\mathrm{d}\tilde{\sigma}_\theta}{\mathrm{d}\rho}(\rho) - \nu\frac{r}{\tau^2}\frac{\mathrm{d}\tilde{\sigma}_r}{\mathrm{d}\rho}(\rho)\right]
\end{aligned} \tag{A4}$$

Replacing these expressions (A4) in the following form of the flow rule below—obtained by elimination of the plastic multiplier:

$$\dot{\varepsilon}_\theta^{\mathrm{p}} = A(\rho\tau,\tau)\dot{\varepsilon}_r^{\mathrm{p}} \tag{A5}$$

where coefficient A stands for

$$A(\rho\tau,\tau) = \left[\frac{\partial g(\sigma_r,\sigma_\theta,\eta)}{\partial\sigma_r}\right]^{-1}\left[\frac{\partial g(\sigma_r,\sigma_\theta)}{\partial\sigma_\theta}\right]$$

The self-similar form of the flow rule is

$$\frac{\mathrm{d}^2\tilde{u}_r}{\mathrm{d}\rho^2} = \frac{1}{\rho}\frac{1}{\tilde{A}}\frac{\mathrm{d}\tilde{u}_r}{\mathrm{d}\rho} - \frac{1}{\rho^2}\frac{1}{\tilde{A}}\tilde{u}_r - \left(\frac{1-\nu}{\tilde{A}} + \nu\right)\frac{\mathrm{d}\tilde{\sigma}_\theta}{\mathrm{d}\rho} + \left(\frac{\nu}{\tilde{A}} + 1 - \nu\right)\frac{\mathrm{d}\tilde{\sigma}_r}{\mathrm{d}\rho} \tag{A6}$$

where coefficient $\tilde{A}$ is

$$\tilde{A} = \left[\frac{\partial g}{\partial \sigma_r}((\sigma^0 - p_i^*)\tilde{\sigma}_\theta, (\sigma^0 - p_i^*)\tilde{\sigma}_r, \tilde{\eta})\right]^{-1}\left[\frac{\partial g}{\partial \sigma_\theta}((\sigma^0 - p_i^*)\tilde{\sigma}_\theta, (\sigma^0 - p_i^*)\tilde{\sigma}_r, \tilde{\eta})\right] \tag{A7}$$

Finally, the persistence equation or plastic activity condition (13) can be written in its self-similar form as

$$\frac{\mathrm{d}\tilde{\sigma}_\theta}{\mathrm{d}\rho} = \frac{1}{\tilde{B}_1}\left[-\tilde{B}_2\frac{\mathrm{d}\tilde{\sigma}_r}{\mathrm{d}\rho} + \frac{1}{2G}\frac{\tilde{B}_3}{\rho^2}\tilde{u}_r - \frac{1}{2G}\frac{\tilde{B}_3}{\rho}\frac{\mathrm{d}\tilde{u}_r}{\mathrm{d}\rho} - \frac{\tilde{B}_4}{2G}\frac{\mathrm{d}^2\tilde{u}_r}{\mathrm{d}\rho^2}\right] \tag{A8}$$

where the presented notation stands as follows:

$$\bar{\sigma}^0 = \frac{\sigma^0 - p_i^*}{2G} \tag{A9}$$

$$\tilde{B}_1 = \frac{\partial f}{\partial \sigma_\theta}((\sigma^0 - p_i^*)\tilde{\sigma}_\theta, (\sigma^0 - p_i^*)\tilde{\sigma}_r, \tilde{\eta}) + \frac{\partial f}{\partial \eta}((\sigma^0 - p_i^*)\tilde{\sigma}_\theta, (\sigma^0 - p_i^*)\tilde{\sigma}_r, \tilde{\eta})$$
$$\frac{\partial \eta}{\partial \sigma_\theta}\left(\bar{\sigma}^0\frac{\tilde{u}_r}{\rho}, \bar{\sigma}^0\frac{\mathrm{d}\tilde{u}_r}{\mathrm{d}\rho}, (\sigma^0 - p_i^*)\tilde{\sigma}_\theta, (\sigma^0 - p_i^*)\tilde{\sigma}_r\right)$$

$$\tilde{B}_2 = \frac{\partial f}{\partial \sigma_r}((\sigma^0 - p_i^*)\tilde{\sigma}_\theta, (\sigma^0 - p_i^*)\tilde{\sigma}_r, \tilde{\eta}) + \frac{\partial f}{\partial \eta}((\sigma^0 - p_i^*)\tilde{\sigma}_\theta, (\sigma^0 - p_i^*)\tilde{\sigma}_r, \tilde{\eta})$$
$$\frac{\partial \eta}{\partial \sigma_r}\left(\bar{\sigma}^0\frac{\tilde{u}_r}{\rho}, \bar{\sigma}^0\frac{\mathrm{d}\tilde{u}_r}{\mathrm{d}\rho}, (\sigma^0 - p_i^*)\tilde{\sigma}_\theta, (\sigma^0 - p_i^*)\tilde{\sigma}_r\right)$$

$$\tilde{B}_3 = \frac{\partial f}{\partial \eta}((\sigma^0 - p_i^*)\tilde{\sigma}_\theta, (\sigma^0 - p_i^*)\tilde{\sigma}_r, \tilde{\eta})\frac{\partial \eta}{\partial \hat{u}_r}\left(\bar{\sigma}^0\frac{\tilde{u}_r}{\rho}, \bar{\sigma}^0\frac{\mathrm{d}\tilde{u}_r}{\mathrm{d}\rho}, (\sigma^0 - p_i^*)\tilde{\sigma}_\theta, (\sigma^0 - p_i^*)\tilde{\sigma}_r\right)$$

$$\tilde{B}_4 = \frac{\partial f}{\partial \eta}((\sigma^0 - p_i^*)\tilde{\sigma}_\theta, (\sigma^0 - p_i^*)\tilde{\sigma}_r, \tilde{\eta})\frac{\partial \eta}{\partial v_r}\left(\bar{\sigma}^0\frac{\tilde{u}_r}{\rho}, \bar{\sigma}^0\frac{\mathrm{d}\tilde{u}_r}{\mathrm{d}\rho}, (\sigma^0 - p_i^*)\tilde{\sigma}_\theta, (\sigma^0 - p_i^*)\tilde{\sigma}_r\right)$$

Equations (A3), (A6) and (A8) can then be expressed in matrix form, as shown in Equation (24) in the main text.

In what concerns the initial conditions required to solve the system by means of the 'ode45' subroutine, the boundary conditions on the elasto-plastic interface presented in Equations (18) should be considered. First, the elastic solution can be re-written in a self-similar form:

$$\tilde{\sigma}_r(\rho) = \tilde{\sigma}^0 - \frac{1}{\rho^2}, \quad \tilde{\sigma}_\theta(\rho) = \tilde{\sigma}^0 + \frac{1}{\rho^2}, \quad \tilde{u}_r(\rho) = \frac{1}{\rho}, \quad \frac{\mathrm{d}\tilde{u}_r(\rho)}{\mathrm{d}\rho} = -\frac{1}{\rho^2} \tag{A10}$$

Then, as the elasto-plastic interface in the self-similar formulation corresponds to $\rho = 1$, the final initial conditions stand:

$$\tilde{\sigma}_r(1) = \tilde{\sigma}^0 - 1, \quad \tilde{\sigma}_\theta(1) = \tilde{\sigma}^0 + 1, \quad \tilde{u}_r(1) = 1, \quad \frac{\mathrm{d}\tilde{u}_r}{\mathrm{d}\rho}(1) = \tilde{v}_r(1) = -1 \tag{A11}$$

In this way the system of ordinary differential equations is formulated according to the self-similarity hypothesis.

APPENDIX B: COEFFICIENTS FOR THE SET OF ORDINARY DIFFERENTIAL EQUATIONS FOR MOHR–COULOMB FAILURE CRITERION AND SIMPLE HYPOTHESES

(a) *Softening regime*:

$$\tilde{B}_1(\rho) = 1 - \frac{1}{2G}\left[2\frac{\phi^{\mathrm{p}} - \phi^{\mathrm{r}}}{\eta^*}\frac{\pi}{180}\frac{\cos\phi(\tilde{\eta})}{(1-\sin\phi(\tilde{\eta}))^2}\left[(\sigma^0 - p_{\mathrm{i}}^*)\tilde{\sigma}_r(\rho) + \frac{C(\tilde{\eta})}{\sqrt{K_{\mathrm{p}}(\tilde{\eta})}}\right] + 2\frac{C^{\mathrm{p}} - C^{\mathrm{r}}}{\eta^*}\sqrt{K_{\mathrm{p}}(\tilde{\eta})}\right] \tag{B1}$$

$$\tilde{B}_2(\rho) = -K_{\mathrm{p}}(\tilde{\eta}) + \frac{1}{2G}\left[2\frac{\phi^{\mathrm{p}} - \phi^{\mathrm{r}}}{\eta^*}\frac{\pi}{180}\frac{\cos\phi(\tilde{\eta})}{(1-\sin\phi(\tilde{\eta}))^2}\left[(\sigma^0 - p_{\mathrm{i}}^*)\tilde{\sigma}_r(\rho) + \frac{C(\tilde{\eta})}{\sqrt{K_{\mathrm{p}}(\tilde{\eta})}}\right] + 2\frac{C^{\mathrm{p}} - C^{\mathrm{r}}}{\eta^*}\sqrt{K_{\mathrm{p}}(\tilde{\eta})}\right] \tag{B2}$$

$$\tilde{B}_3(\rho) = 2\frac{\phi^{\mathrm{p}} - \phi^{\mathrm{r}}}{\eta^*}\frac{\pi}{180}\frac{\cos\phi(\tilde{\eta})}{(1-\sin\phi(\tilde{\eta}))^2}\left[(\sigma^0 - p_{\mathrm{i}}^*)\tilde{\sigma}_r(\rho) - \frac{C(\tilde{\eta})}{\sqrt{K_{\mathrm{p}}(\tilde{\eta})}}\right] + 2\frac{C^{\mathrm{p}} - C^{\mathrm{r}}}{\eta^*}\sqrt{K_{\mathrm{p}}(\tilde{\eta})} \tag{B3}$$

$$\tilde{B}_4(\rho) = -\tilde{B}_3(\rho) \tag{B4}$$

(b) *Residual regime*:

$$\tilde{B}_1(\rho) = 1 \tag{B5}$$

$$\tilde{B}_2(\rho) = -K_{\mathrm{p}}(\tilde{\eta}) \tag{B6}$$

$$\tilde{B}_3(\rho) = \tilde{B}_4(\rho) = 0 \tag{B7}$$

APPENDIX C: COEFFICIENTS FOR THE SYSTEM OF ORDINARY DIFFERENTIAL EQUATIONS FOR HOEK–BROWN CRITERION

(a) *Softening regime*:

$$\tilde{A}(\rho) = -\frac{1}{K(\tilde{\eta})} \tag{C1}$$

$$\tilde{B}_1(\rho) = 1 - \frac{1}{2G}\frac{\partial F}{\partial \eta}(X_1(\rho), X_2(\rho), X_3(\rho)) \tag{C2}$$

$$\tilde{B}_2(\rho) = -1 - \frac{m(\tilde{\eta})\sigma_{ci}}{2\sqrt{m(\tilde{\eta})\sigma_{ci}(\sigma^0 - p_i^*)\tilde{\sigma}_r(\rho) + s(\tilde{\eta})\sigma_{ci}^2}} + \frac{1}{2G}\frac{\partial F}{\partial \eta}(X_1(\rho), X_2(\rho), X_3(\rho)) \tag{C3}$$

$$\tilde{B}_3(\rho) = \frac{\partial F}{\partial \eta}(X_1(\rho), X_2(\rho), X_3(\rho)) \tag{C4}$$

$$\tilde{B}_4(\rho) = -\frac{\partial F}{\partial \eta}(X_1(\rho), X_2(\rho), X_3(\rho)) \tag{C5}$$

where

$$\frac{\partial F}{\partial \eta}(X_1(\rho), X_2(\rho), X_3(\rho)) = -\frac{(\sigma^0 - p_i^*)\tilde{\sigma}_r(\rho)\sigma_{ci}\dfrac{dm}{d\eta}(\tilde{\eta}) + \sigma_{ci}^2\dfrac{ds}{d\eta}(\tilde{\eta})}{2\sqrt{m(\tilde{\eta})(\sigma^0 - p_i^*)\tilde{\sigma}_r(\rho)\sigma_{ci} + s(\tilde{\eta})\sigma_{ci}^2}} \tag{C6}$$

$$\frac{\partial F}{\partial \eta}(X_1(\rho), X_2(\rho), X_3(\rho)) = \frac{(\sigma^0 - p_i^*)\tilde{\sigma}_r(\rho)\sigma_{ci}\dfrac{m^p - m^r}{\eta^*} + \sigma_{ci}^2\dfrac{s^p - s^r}{\eta^*}}{2\sqrt{m(\tilde{\eta})(\sigma^0 - p_i^*)\tilde{\sigma}_r(\rho)\sigma_{ci} + s(\tilde{\eta})\sigma_{ci}^2}} \tag{C7}$$

(b) *Residual regime*:

$$\tilde{B}_1(\rho) = 1 \tag{C8}$$

$$\tilde{B}_2(\rho) = -1 - \frac{m^r\sigma_c}{2\sqrt{m^r\sigma_{ci}(\sigma^0 - p_i^*)\tilde{\sigma}_r(\rho) + s^r\sigma_{ci}^2}} \tag{C9}$$

$$\tilde{B}_3(\rho) = \tilde{B}_4(\rho) = 0 \tag{C10}$$

REFERENCES

1. Pacher F. Deformationsmessungen in Versuchsstollen als Mettel zur Erforschung des Gebirgsverhaltens und zur Bemessung des Ausbaues. *Felsmechanik und Ingenieurgeologie* 1964; **2**:149–161.
2. Panet M. Understanding deformations in tunnels. In *Comprehensive Rock Engineering*, Hudson (ed.), vol. I. Pergamon Press: Oxford, 1993; 663–690.
3. Panet M. *Le calcul des tunnels par la méthode des curves convergence–confinement*. Presses de l'École Nationale des Ponts et Chaussées: Paris, 1995.
4. Salençon J. Contraction quasistatique d'une cavité à symètrie sphérique ou cylindrique dans un milieu elastoplastique. *Annales des Ponts et Chaussées* 1969; **4**:213–236.
5. Fairhurst Ch. General philosophy of support design for underground structures in hard rock. In *Underground Structures: Design and Construction. Developments in Geotechnical Engineering Series*, Sinha S (ed.), vol. 59B. Elsevier: Amsterdam, 1991.
6. Hoek E, Kaiser PK, Bawden WF. *Support of Underground Excavations in Hard Rock*. Balkema: Rotterdam, 1995.
7. Carranza-Torres C, Fairhurst C. The elasto-plastic response of underground excavations in rock masses that obey the Hoek–Brown failure criterion. *International Journal of Rock Mechanics Sciences and Geomechanics Abstracts* 1999; **36**(5):777–809.
8. Eberhart E. Numerical modelling of three-dimension stress rotation ahead of an advancing tunnel face. *International Journal of Rock Mechanics and Mining Sciences* 2000; **38**:499–518.
9. Hoek E. Rock Engineering. Course notes in page, http://www.rocscience.com. [pp. 204–214] (07/11/2000).
10. Carranza-Torres C. Self similarity analysis of the elastoplastic response of underground openings in rock and effects of practical variables. *Ph.D. Thesis*, University of Minnesota, 1998.

11. Hoek E, Brown ET. Practical estimates of rock mass strength. *International Journal of Rock Mechanics Sciences and Geomechanics Abstracts* 1997; **34**(8):1165–1187.
12. Hudson JA, Brown ET, Fairhurst C. Shape of the complete stress–strain curve for rock. *Proceedings of the 13th Symposium on Rock Mechanics*, University of Illinois, 1971.
13. Kimura T, Esaki T, Kameda N, Nishida T. Experimental and theoretical studies on strain softening behaviour of rocks. *28th US Symposium on Rock Mechanics*, Tucson, 1987; 197–2002.
14. Read HE, Hegemeier GA. Strain softening of rock, soil and concrete—a review article. *Mechanics and Materials* 1984; **3**:271–294.
15. Sture S, Ko HY. Strain-softening of brittle geologic materials. *International Journal of Numerical and Analytical Methods in Geomechanics* 1978; **2**:237–253.
16. Bieniawski ZT. Rock mass classification in rock engineering. *Proceedings, Symposium on Exploration for Rock Engineering*, Johannesburg, vol. 1, 1976; 97–106.
17. Egger P. Design and construction aspects of deep tunnel (with particular emphasis on strain softening rocks). *Tunnelling and Underground Space Technology* 2000; **15**(4):403–409.
18. Schwartz CW, Einstein HH. Simplified analysis for ground-structure interaction in tunnelling. The state of the art in Rock Mechanics. *Proceedings of the 21st U.S. Symposium on Rock Mechanics*, University of Missouri-Rolla, 1980; 787–796.
19. Ladanyi B. Use of the long-term strength concept in the determination of ground pressure on tunnel linings. In *Advances in Rock Mechanics, Proceedings of the 3rd Congress of the International Society for Rock Mechanics*, vol. 2, No. B. National Academy of Sciences: Washington, DC, 1974; 1150–1156.
20. Hoek E, Brown ET. *Underground Excavations in Rock*. Champan & Hall: London, 1980.
21. Wang Y. Ground response of circular tunnel in poorly consolidated rock. *Journal of Geotechnical Engineering* 1996; **122**(9):703–708.
22. Brown ET, Bray JW, Ladanyi B, Hoek E. Ground response curves for rock tunnels. *Journal of Geotechnical Engineering* 1983; **109**(1):15–39.
23. Duncan Fama ME. Numerical modelling of yield zones in weak rock. In *Comprehensive Rock Engineering*, Hudson J (ed.), vol II. Pergamon Press: Oxford, 1993; 49–75.
24. Gumusoglu MC, Bray JW, Watson JO. Analysis of underground excavations incorporating the strain softening of rock masses. *Proceedings of the 6th International Congress of the ISRM*, vol. 2, Aachen, 1987; 923–928 (in Germany).
25. Charlez A. *Rock Mechanics. Theoretical Fundamentals*, vol. 1. Technip: Paris, 1991.
26. Hill R. *The Mathematical Theory of Plasticity*. Oxford University Press: New York, 1950.
27. Halphen B, Salençon J. *Elastoplasticité*. Presses de L'École Nationale des Ponts et Chaussées, Paris, 1987.
28. Kaliszky S. *Plasticity: Theory and Engineering Applications*. Elsevier: Amsterdam, 1989.
29. Duncan Fama ME, Trueman R, Craig MS. Two and three dimensional elastoplastic analysis for coal pillar design and its application to highwall-mining. *International Journal of Rock Mechanics Sciences and Geomechanics Abstracts* 1995; **32**(3):215–225.
30. Vermeer PA, De Borst R. *Non associated plasticity for soils, concrete and rock*. Heron 1984; **29**(3):3–64.
31. Itasca. *User manual for FLAC, Version 3.4*. Itasca Consulting Group Inc.: Minnesota, 1998.
32. Vardoulakis IG, Sulem J. *Bifurcation Analysis in Geomechanics*. Blackie Academic & Professional: London, 1995.
33. Pethukov IM, Linkov AM. The theory of post-failure deformation and the problem of stability in rock. *International Journal of Rock Mechanics Sciences and Geomechanics Abstracts* 1979; **16**:17–56.
34. Medhurst TP, Brown ET. A study of the mechanical behaviour of coal for pillar design. *International Journal of Rock Mechanics Sciences and Geomechanics Abstracts* 1998; **35**(8):1087–1105.
35. Brady BHG, Brown ET. *Rock Mechanics for Underground Mining* (2nd edn). Chapman & Hall: London, 1993.
36. Alonso E. Ground reaction curves: numerical resolution and application to strain-softening rock masses. *Ph.D. Thesis*, Department of Natural Resources and Environmental Engineering, University of Vigo, 2002 (in Spanish).
37. Detournay E. Two dimensional elastoplastic analysis of a long, cylindrical cavity under non hydrostatic loading. *Ph.D. Thesis*, University of Minnesota, 1983.
38. Bigoni D. Bifurcation and instability of non-associative elastoplastic solids. In *Material Instabilities in Elastic and Plastic Solids*. Lectures at CISM, Udine, Italy, September 13–17, 1999, Petryk H (ed.). Springer: Wien, CISM Courses Lecture, vol. 414, 2000; 1–52; MSC 2000.
39. Varas F, Alonso E, Alejano LR, Fdez.-Manín G, Carranza-Torres C. Study of bifurcation in the problem of axi-symmetric unloading of a circular excavation in a strain-softening material, in preparation.
40. Dormand JR, Prince PJ. A Family of embedded Runge–Kutta formulae. *Journal of Computational and Applied Mathematics* 1980; **6**:19–26.
41. Brown ET, Bray JW, Santarelli FJ. Influence of stress-dependent elastic moduli on stresses and strains around axisymmetric boreholes. *Rock Mechanics and Rock Engineering* 1989; **22**:189–203.

42. Wilson AH. Research into the determination of pillar size (Part 1: an hypothesis concerning pillar stability). *Transactions of the Institution of Mining Engineers* 1972; **131**:409–417.
43. Alejano LR, Ramírez-Oyanguren P, Taboada J. FDM predictive methodology of subsidence due to flat and inclined coal seam mining. *International Journal of Rock Mechanics Sciences and Geomechanics Abstracts* 1999; **36**(4): 475–491.
44. Carranza-Torres C, Alonso E, Alejano LR, Varas F, Fdez.-Manín G. Elasto-plastic analysis of deep tunnels in brittle rock using a scaled form of the Mohr–Coulomb failure criterion. In Hammah *et al.* (eds), *Proceedings of NARMS-TAC. 2002*, Mining Innovation and Opportunity, vol. 1. University of Toronto Press: Toronto, 2002; 283–296.
45. Alejano LR, Alonso E, Fdez-Manín G, Varas F. Numerical solution of ground reaction curves by means of self-similar solutions. *Proceedings of Vth National Congress of Numerical Methods in Engineering*, Madrid, Spain, 2002 (in Spanish).

